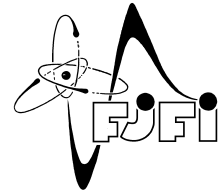




CZECH TECHNICAL UNIVERSITY IN PRAGUE
Faculty of Nuclear Sciences and Physical
Engineering



Adiabatic transitions in discrete-time systems

Adiabatické přechody v časově diskrétních systémech

Master's thesis

Author: **Filip Němec**
Supervisor: **Ing. Václav Potoček, Ph.D.**
Year: 2020/2021

Acknowledgement:

I would like to offer my thanks to Ing. Václav Potoček, Ph.D., supervisor of my thesis, for his guidance, his inspiring remarks and comments. His proposals and ideas inspired me significantly. Conversations with Václav were always of great help to me. I am particularly grateful to my family: I would not be able to complete this task without their support. Nobody has been more important in this pursuit than Káťa.

Čestné prohlášení:

Prohlašuji, že jsem tuto práci vypracoval samostatně a uvedl jsem všechnu použitou literaturu.

V Praze dne 19.05.2021

Filip Němec

Název práce: **Adiabatické přechody v časově diskrétních systémech**

Autor: Filip Němec

Obor: Matematická fyzika

Druh práce: Diplomová práce

Vedoucí práce: Ing. Václav Potoček, Ph.D., Katedra fyziky Fakulty jaderné a fyzikálně inženýrské ČVUT v Praze

Abstrakt: Zabýváme se jednorozměrnou Hadamardovou procházkou na nekonečné diskrétní síťce. Její prostorová homogenita může být narušena: například defekty v mincovém prostoru. V této práci představíme analytické řešení problému vlastních čísel Hadamardovy procházky s jedním mincovým defektem. Dále uvedeme konečnou analogii zkoumaného systému a zavedeme patřičné okrajové podmínky. Přestože se spektrální vlastnosti obou modelů značně liší, podléhají při perturbacích jejich spektra překvapivě podobnému vývoji. Této vlastnosti lze s výhodou využít, neboť můžeme ve finitním případě numericky zkoumat situace, jež analyticky řešit neumíme. Ze spektrálních vlastností konečného perturbovaného systému pak můžeme usuzovat na vlastnosti spekter nekonečných procházek. Tento postup je vhodný pro analýzu adiabatických přechodů mezi více mincovými defekty.

Klíčová slova: Kvantové procházky, Hadamardova procházka, adiabatický přechod, mincový defekt, perturbace, simulace kvantových procházek, vázané stavy.

Title: **Adiabatic transitions in discrete-time systems**

Author: Filip Němec

Supervisor: Ing. Václav Potoček, Ph.D., Department of Physics, Faculty of Nuclear Sciences and Physical Engineering, Czech Technical University in Prague

Abstract: We consider a one-dimensional Hadamard walk on an infinite lattice. Its space homogeneity may be disturbed by various coin defects. We provide an analytical solution to the eigenvalue problem for a general single-poin defect. We also provide a comparison with a finite model of the Hadamard walk. While the finite and infinite model have significantly different spectral properties, their behaviour under coin perturbations is strikingly similar. This property is to our benefit, for we may numerically simulate cases with no known analytical solution and infer spectral properties of walks on infinite grids. This method is particularly useful while examining adiabatic transitions between multiple coin perturbations.

Key words: Quantum walks, Hadamard walk, adiabatic transition, coin defect, perturbation, simulation of quantum walks, trapped states.

Contents

1	Introduction, basic concepts	2
1.1	Random walks in the quantum realm	2
1.2	From Quantum Computing to Adiabatic Theorem	6
1.3	Adiabatic theorems of quantum mechanics	8
2	The Hadamard walk	12
2.1	Finite-dimensional case and additional boundary conditions	14
2.2	Analysis of coin-space defects	16
2.2.1	Known cases	17
2.3	Eigenvalue problem for general coin defects	19
2.4	Phase-altered Hadamard coin and rotations revisited	28
2.5	Possible generalizations	29
3	Numerical solutions for the Hadamard walk	33
3.1	Outline of the simulation	33
3.2	Adiabatic transitions	35
3.3	Perturbation shift	40
4	Conclusion	47
A	Appendix	48
A.1	Minor implementation details	48

1 Introduction, basic concepts

Ever since the the beginning of ages people have been puzzled by the world that surrounds us. Every human epoch carries topics of peoples' interest; the more we know, the broader our interests are. Once upon the time we experience both puzzling and illuminating breakthrough such as discoveries of quantum mechanics, special relativity or computer sciences. For some times, people tend to find connections between such topics, try to combine them and derive new and more general concepts.

In this thesis, we introduce Hadamard walk on an infinite discrete line and also its finite analogue. One of the key properties of such walks is their spatial homogeneity. We will, however, investigate small perturbations in their structure and regard the impact on their spectra. Such structure-preserving perturbations are known as coin defects[1]. We shall derive an analytical solution to the eigenvalue problem of the Hadamard walk with a general single-point defect. Even though spectral properties of the finite and infinite models differ significantly,we uncover a surprisingly similar behaviour with respect to the coin perturbations. Although we are able to find stationary states of Hadamard walks with a single defect, we are not able to analyze multiple coin defects analytically. This is unfortunately the case that arise during various transitions between perturbations. We might, for example, trap a walker at a desired location using a phase-altered coin [2]. If we were to move the localized walker, we need to somehow shift the coin defect the walker is attracted to. We might encounter a co-existence of two structural perturbations in the close vicinity during the transition. Despite not being able to examine these transitions analytically we can examine them using the finite model. Even though its spectrum differs fundamentally, both models share strikingly similar behaviour while undergoing perturbations. We thus implemented own framework in order to simulate adiabatic transitions and provide several examples concerning different coin defects.

We shall at first introduce the Hadamard walk and its structure. An impact of single-point perturbations on the stationary states will be discussed in Section 2.2. We begin by presenting known examples and then add our own solution to the single coin defect problem. Later on, in Section 3.1 a short note on methods and techniques used in our simulation framework will be provided. This section also includes the examples of adiabatic transitions in different settings.

1.1 Random walks in the quantum realm

We begin by introducing a classical random walk. At first, a model for discrete classical walks will be discussed [3]. We imagine a walker or a particle located in a state space. The walker performs steps in the state space and our task is to examine the resulting paths. In this example the evolution takes place in an infinite grid \mathbb{Z}^d where \mathbb{Z} denotes the set of integers. The state space is equipped with a *transition function* $P : \mathbb{Z}^d \times \mathbb{Z}^d \rightarrow \mathbb{R}_+$ satisfying:

$$(\forall x, y \in \mathbb{Z}^d) (P(x, y) = P(0, x - y)), \quad (1)$$

$$(\forall x, y \in \mathbb{Z}^d) \left(\sum_{x \in \mathbb{Z}^d} P(0, x) = 1 \right). \quad (2)$$

The transition function dictates the probability of transition from a point x to a point y in a single step of the walk. The first equation postulates spatial homogeneity and the

second postulates the normalisation of probability. We may imagine a random walker placed on a grid whose only task is to move according the transition function at each time step. No matter where he stands at a particular time the transition function does not change thanks to the spatial homogeneity.

A well-known example is that of a *simple random walk*. We shall denote the d -dimensional Euclidean norm by $\|x\| = \sqrt{\sum_{i=1}^d (x_i)^2}$, where x_i denotes the i -th coordinate of x . Define the transition function as follows:

$$P(0, x) = \frac{1}{2d} \quad \text{if} \quad \|x\| = 1, \quad (3)$$

$$P(0, x) = 0 \quad \text{if} \quad \|x\| \neq 1. \quad (4)$$

This choice of the transition function ensures that the probability of finding the walker somewhere in the grid remains constant.

In the case $d = 1$ when the state space is a discretized line standing at the point 0 the walker has two directions to choose from. The transition function (4) implies that the walker certainly does not stay at position 0 and that the probabilities of choosing either left or right direction are equal. The same reasoning holds for higher dimensions as well: any point in \mathbb{Z} has $2d$ direct neighbours.

A simple physical model of a one-dimensional random walk may be constructed. Imagine we stuck pins onto a board as depicted in figure 1. If we lift the top of the board keeping the base placed on the floor, so that marbles can roll down from the top vertex, each pin forces marbles to go either left or right at random. In the ideal case, the probabilities are both equal to $\frac{1}{2}$ but we might slightly tilt the board to achieve a biased walk. If we lift one side of the base just slightly, all marbles are forced to prefer one direction. ¹

An observer measures positions where marbles leave the board. Having done multiple experiments, one finds that for both biased and unbiased walks, the resulting distribution resembles the binomial distribution.

An ideal model of the latter board is mathematically described as n independent Bernoulli trials, where n stands for the number of layers of nails (for the case in Figure 1 $n = 5$).

¹We neglect momenta of the marbles. In the real world, these aspects might cause non-Markovian behavior. [4]

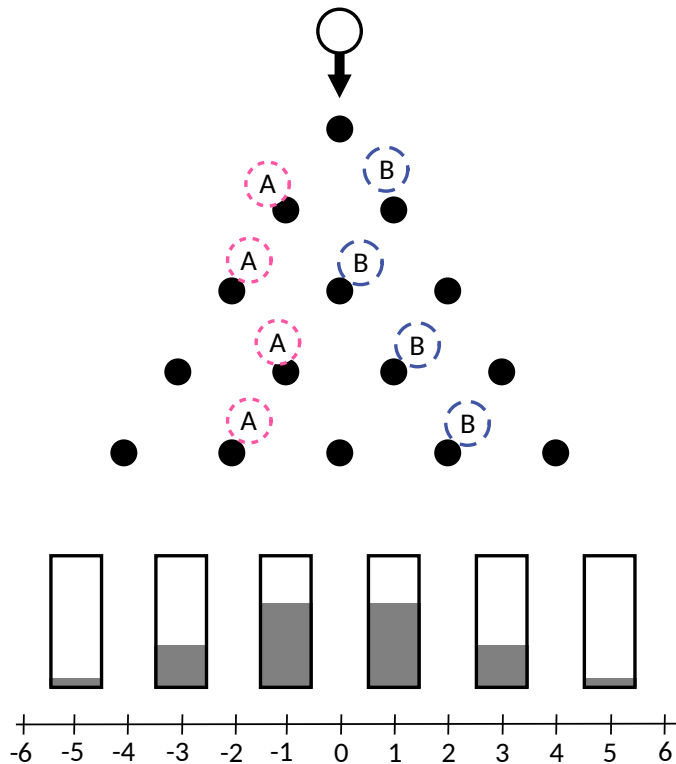


Figure 1: Galton's board (Quincunx) with sample trajectories of two marbles. We let the marbles fall from top of the board. Clearly, for $n = 5$ layers, only odd positions are allowed as results. The bins to collect escaping balls are thus placed only at odd positions. Additionally, grey bars indicate the resulting distribution for a very high number of trials; the full height of a slot is scaled to probability $\frac{1}{2}$.

In 1993, Y. Aharonov, L. Davidovich and N. Zagury [5] investigated a quantum analogy to the classical random walks. Their concept used a spin- $\frac{1}{2}$ particle located on a 1-dimensional line. Imagine there is a particle localized at point x_0 having spin $c_-|\uparrow\rangle + c_+|\downarrow\rangle$ and denote its state $(c_-|\uparrow\rangle + c_+|\downarrow\rangle)|\psi(x_0)\rangle$. We use column vector notation:

$$|\uparrow\rangle = \begin{pmatrix} 1 \\ 0 \end{pmatrix}, \quad |\downarrow\rangle = \begin{pmatrix} 0 \\ 1 \end{pmatrix} \quad (5)$$

for a description of the spin-space using S_z eigenvectors, where

$$S_z = \frac{\hbar}{2} \begin{pmatrix} 1 & 0 \\ 0 & -1 \end{pmatrix} = \frac{\hbar}{2} (|\uparrow\rangle\langle\uparrow| - |\downarrow\rangle\langle\downarrow|) \quad (6)$$

denotes spin projection along z axis.

Denoting the momentum operator P , one may express translation to a step of length l as follows:

$$I \otimes T_l(c_-|\downarrow\rangle + c_+|\uparrow\rangle)|\psi(x_0)\rangle = I \otimes \exp\left(-\frac{i}{\hbar}Pl\right) (c_-|\downarrow\rangle + c_+|\uparrow\rangle)|\psi(x_0)\rangle = \quad (7) \\ (c_-|\downarrow\rangle + c_+|\uparrow\rangle)|\psi(x_0 - l)\rangle,$$

where $|\psi(x_0 - l)\rangle$ represents a wave packet centered around $x_0 - l$. Note that the translation chosen in (7) acts trivially on the spin space. What if we try to construct a

conditional transition that moves the particle based on its spin?

$$\begin{aligned}
& \left[(|\uparrow\rangle\langle\uparrow|) \otimes \exp\left(-\frac{i}{\hbar}Pl\right) + (|\uparrow\rangle\langle\uparrow|) \otimes \exp\left(\frac{i}{\hbar}Pl\right) \right] (c_-|\downarrow\rangle + c_+|\uparrow\rangle)|\psi(x_0)\rangle = \\
& c_-|\downarrow\rangle \otimes \exp\left(-\frac{i}{\hbar}Pl\right)|\psi(x_0)\rangle + c_+|\uparrow\rangle \otimes \exp\left(\frac{i}{\hbar}Pl\right)|\psi(x_0)\rangle = \\
& c_-|\downarrow\rangle|\psi(x_0-l)\rangle + c_+|\uparrow\rangle|\psi(x_0+l)\rangle = U_l(c_-|\downarrow\rangle + c_+|\uparrow\rangle)|\psi(x_0)\rangle.
\end{aligned} \tag{8}$$

Such spin-conditioned transition U_l will enable us to create a quantum analogy of classical random walks. But at first imagine the examined particle happens to have internal spin that is an eigenstate of S_z , for example $|\downarrow\rangle|\psi(x_0)\rangle$. Then the evolution dictated by the effective evolution operator U_l from the equation (8) forces the particle to move left by l in each step. Such a walk is not really a random walk. On the other hand it enables us to mimic translations defined by the equation (7). More interesting behavior may be observed when considering particles with internal spin that is a superposition of $|\downarrow\rangle, |\uparrow\rangle$.

1. Having begun with state $\Psi_0 = (c_-|\downarrow\rangle + c_+|\uparrow\rangle)|\psi(x_0)\rangle$ we apply the conditional transition operator (8); the resulting state will be: $\Psi_1 = c_-|\downarrow\rangle|\psi(x_0-l)\rangle + c_+|\uparrow\rangle|\psi(x_0+l)\rangle$.
2. Performing a measurement of the spin on $\tilde{\Psi}_1$, we either find spin $-\frac{\hbar}{2}$ with probability $|c_-|^2$ and the particle will be located at x_0-l , or we measure spin $\frac{\hbar}{2}$ with probability $|c_+|^2$ and the particle will be at x_0+l .
3. Suppose, for example, spin $-\frac{\hbar}{2}$ and thus position x_0-l was measured. Provided we then prepare a new state $\tilde{\Psi}_1 = (c_-|\downarrow\rangle + c_+|\uparrow\rangle)|\psi(x_0-l)\rangle$, we apply the conditional step and measure the spin again, either $c_-|\downarrow\rangle|\psi(x_0-2l)\rangle$ or $c_+|\uparrow\rangle|\psi(x_0)\rangle$ are obtained.
4. Repeating this procedure one is fully capable to mimic classical random walk on a line.

Returning to the equation (8) describing the effective evolution operator for a single conditional step, we may write [1]:

$$U_l = \left[(|\uparrow\rangle\langle\uparrow|) \otimes \exp\left(-\frac{i}{\hbar}Pl\right) + (|\uparrow\rangle\langle\uparrow|) \otimes \exp\left(\frac{i}{\hbar}Pl\right) \right] = \tag{9}$$

$$\exp\left(-\frac{i}{\hbar}(|\uparrow\rangle\langle\uparrow| - |\downarrow\rangle\langle\downarrow|) \otimes Pl\right) = \exp\left(-2\frac{i}{\hbar}S_z \otimes Pl\right), \tag{10}$$

since $|\downarrow\rangle\langle\downarrow|$ and $|\uparrow\rangle\langle\uparrow|$ are projections and any natural power leaves them unaffected, and because operators $|\downarrow\rangle\langle\downarrow| \otimes P$ and $|\uparrow\rangle\langle\uparrow| \otimes P$ commute. We have arrived at the same form of unitary evolution as described in [5].

From now on, let \hbar be equal to 1; such a choice simplifies the equations without introducing any ambiguity.

Note 1.1. Up until now we have discussed our ability to replicate classical biased walks on a line using equation (8) or (9). There are several questions to be answered:

1. Does the quantum analogy bring any new phenomena?

2. Is there a quantum analogy to classical walks on lattices?
3. Since we know classical walks may be used as a building block for designing certain algorithms, could we use quantum walks for quantum computation? And if yes, do we gain any speedup against classical computation?

1.2 From Quantum Computing to Adiabatic Theorem

For a physicist the possibility of being able to effectively simulate evolution of a physical system has always been an important question. Predictions of classical physics are based on ordinary and partial differential equations, finding extremes of certain functionals etc. Digital computers play a major role in the world of simulation because classical analog computers are not very suitable for such task. They require extremely precise setting and control over external conditions (baths, shielding, mechanical isolation etc.) in order to provide sufficiently reliable results. Moreover their setting is very subtle and we are often unable to gather precise control over all components (e.g. due to noise) [6]. The idea of using physical phenomena reappeared in Feynman's article from 1982 [7] where he suggested performing simulations of quantum systems using other quantum systems.

From the perspective of computer scientists, the circuit model of quantum computation has been theoretically examined as the first universal model of quantum computing [8], [9] and [10]. Computations are performed in the domain of the circuit model using unitary gates that operate on qubits [11]. Processors used in digital computers implement only particular subsets of all possible logical operations from which more complex instructions are composed [12]. Despite this, we are able to show that they may perform any logical operation desired; this property is called universality [6], [13]. A similar result is known for the circuit model: any unitary operation may be expressed using Hadamard gate H , phase gate S , $\pi/8$ gate T and CNOT gate to arbitrary accuracy [11]. These gates are expressed by matrices:

$$H = \frac{1}{\sqrt{2}} \begin{pmatrix} 1 & 1 \\ 1 & -1 \end{pmatrix}, \quad S = \begin{pmatrix} 1 & 0 \\ 0 & i \end{pmatrix}, \quad (11)$$

$$T = \begin{pmatrix} 1 & 0 \\ 0 & e^{i\pi/4} \end{pmatrix}, \quad \text{CNOT} = \begin{pmatrix} 1 & 0 & 0 & 0 \\ 0 & 1 & 0 & 0 \\ 0 & 0 & 0 & 1 \\ 0 & 0 & 1 & 0 \end{pmatrix}. \quad (12)$$

An alternative approach to quantum computing uses an encoding of computationally hard problems as a ground state of a specifically designed Hamiltonians. Imagine we are able to map an output of an algorithm as a ground state of H_1 and that we find a Hamiltonian H_0 with known ground state and a deformation of H_0 to H_1 . Provided that the transition between Hamiltonians is slow enough and we do not change the degeneracy of the ground state during the transition, we might end up with the ground state of H_1 . This idea is formally governed by adiabatic theorems of the quantum mechanics. There are several versions and each is suitable under different circumstances; discussion of adiabatic theorems is left to the section 1.3.

The design of encoding a result of a computation as a ground state appeared in 1988 [14] in the article Quantum Stochastic Optimization written by Apolloni, Carvalho, and de Falco [15]. Their approach was later considered as a branch of quantum annealing

(QA) [14]. QA was understood as a quantum counterpart to the simulated annealing [16]. Later, in 1999, Brooke et al. published an article Quantum Annealing of a Disordered Magnet where they investigated an implementation of QA in experimental configurations of disordered quantum ferromagnets. Their experiments provided a step towards construction of devices enabling to perform QA and this approach became interesting from the perspective of the quantum computing [14]. In 2000 Farhi et. al. proposed a solution of SAT-3 problem based on a quantum adiabatic algorithm [17]. The term adiabatic quantum computing (AQC) was introduced by van Dam, Mosca and Vazirani at Symposium on Foundations of Computer Science in 2001 [18], [14].

In 2007 Aharonov et. al. [19] found connections of computation resources between the adiabatic and the circuit paradigms: they showed that we are able to simulate AQC using the circuit model and vice versa with only a polynomial overhead. They also stated a precise definition of AQC using k -local Hamiltonians [19].

Definition 1.1. We say that a hermitian matrix H acting on a space of p -state particles (e.g. binary particles) that may be written as $H = \sum_{i=1}^r H_i$, where each H_i acts non-trivially on at most k particles, is a k -local Hamiltonian. We suppose that $p \geq 2$.

The adiabatic quantum computing is defined as follows [19].

Definition 1.2. A k -local adiabatic quantum computation is specified by two k -local Hamiltonians H_0 and H_1 acting on p -state particles and by a description of the adiabatic evolution. We pose additional conditions on the Hamiltonian: the ground state of H_0 is unique and it is a product state. The adiabatic evolution is described by a constant T : total runtime and time-evolution function $s(t) : [0, T] \rightarrow [0, 1]$, an increasing smooth bijection.

We set the time dependent Hamiltonian $H(s)$ to be

$$H(s) = (1 - s)H_0 + sH_1.$$

Both T and $s(t)$ have to be adjusted in such way that the final state of the adiabatic evolution generated by $H(s) = (1 - s)H_0 + sH_1$ at time T , $|\psi(T)\rangle$, is ε -close in L^2 norm to the ground state of H_1 , say $|\varphi\rangle$: $\| |\varphi\rangle - |\psi(T)\rangle \| < \varepsilon$, where ε is a parameter from $(0, 1]$ describing the precision of our computation.

The output of the adiabatic computation is the evolved vector $|\psi(T)\rangle$.

Note 1.2. A few comments to the latter definition 1.2:

1. If the function $s(t)$ is given, ε can be calculated (for example as an estimate on the computation error). Usually, in practice, however, one would like to perform a calculation and given a parameter $\varepsilon \in (0, 1]$ design the evolution function $s(t)$.
2. Even though the definition 1.2 supposes non-degenerate ground states of the Hamiltonian $H(s)$, we may suppress this assumption, for the adiabatic theorem of the quantum mechanics holds also for degenerate spectra (but it is necessary to track the path not of eigenvector but rather that of the whole eigenspace belonging to the lowest energy). Nevertheless Aharonov showed in [19] that the simpler case is sufficient in order to obtain a computation model of the equal strength as the quantum circuit model.

3. The definition 1.2 supposes that only the evolution of the ground state is tracked. In practise it may be useful to track the evolution of excited states (e.g. the glued trees problem [20], [21]). Although, strictly speaking, such a computation does not belong to the class AQC defined 1.2, it is generally considered as a variation on AQC.
4. The evolution given by 1.2 is not the most general. In fact, there are known situations in which a different type is needed. Aharonov proposed introducing an *intermediate catalyst* – a Hamiltonian $H_c(s)$ depending on $s \in [0, 1]$ that satisfies: $H_c(0) = H_c(1) = 0$ [19]. Having introduced the catalyst Hamiltonian, we may be able to guarantee non-degeneracy of the first two eigenvalues from the spectrum of $H(s) := (1 - s)H_0 + sH_1 + H_c(s)$ despite the fact that the ground eigenvalues of $H(s) := (1 - s)H_0 + sH_1$ would become degenerate during the evolution.

Farhi et. al. investigated the use of an intermediate catalyst in the article Quantum computation by adiabatic evolution [17] while solving the SAT-3 problem with use of the adiabatic evolution.

5. An intuitive way to understand the value of k may be that it somehow manages the interconnection between degrees of freedom of the given system. In this sense it may be compared to memory requirements from the classical computing theory. During the time there has always been investigation of the value k and its relation to computation resources. In 2007 Aharonov et. al. showed that $k = 6$ suffices to create a universal AQC. It is also known that such k has to be at least 2, see [22] and [23].

Further details concerning the history of our knowledge regarding the impact of k to computation resources are summarized in [14]

1.3 Adiabatic theorems of quantum mechanics

In 1916 Ehrenfest stated a hypothesis that the laws of quantum physics would allow only certain motions. He supposed that evolution governed by the quantum mechanics might be invariant under slowly introduced perturbations – adiabatic perturbations [24]. The idea was later investigated by Born and Fock. They studied adiabatic changes of operators with discrete spectra [25]. Later, in 1950, Kato expanded the class of operators to be considered and stated a rigorous version of the adiabatic theorem (AT) governing both operators with discrete spectra and operators with non-discrete or possibly degenerate spectra [26]. However, we need to encompass an important property operators, whose evolution is to be examined, should have. When we imagine an adiabatic transition we usually tend to fix a final state that is to be achieved by end of the transition. The requirement for a suitable “consolidation” is discussed in [27]. Although Kato did not use this definition in the statement of the adiabatic theorem, he implicitly assumed that investigated evolution *consolidate* in the proof. This assumption is necessary because we may derive counterexamples of Hamiltonians with oscillatory driving terms whose evolution is very slow – and are admitted by the Kato’s statement of the AT – but they never reach a final fixed state. Furthermore there are counterexamples that satisfy the requirements imposed by Kato but violating the statement of AT. For a summary of comments on Kato’s proof, examples of Hamiltonians with oscillatory driving terms and other remarks see [27].

We begin by introducing so-called “approximate” versions ² of the AT. We used the attribute “approximate” because additional assumptions have to be added in order to make the statements valid, to be more precise to disallow certain pathological cases. For a critique of different versions of the AT see for example [27], [28] or [29]. Although there are known refinements of these “approximate” versions, their statements are cumbersome and complicated. In practice, the *approximate* versions of the AT often hold: for example when we slowly introduce a perturbation or in AQC. While designing algorithms, we usually tend to find an ingenious way to perform a deformation of the system under consideration without introducing unnecessary disturbances or even oscillatory driving terms which are the typical counterexamples to the validity of AT. Another rationale why to start with the “approximate” statements is that historically they came first and the refined rigorous versions of the AT are usually based on them.

Born’s and Fock’s statement of the AT concerned Hamiltonians with discrete and non-degenerate spectra. Later, Messiah presented a generalised version for Hamiltonians with possibly degenerate spectra in his monograph Quantum Mechanics [30]. Both statements are analogous except for the degeneracy. Denote the instantaneous eigenstates of a time-dependent Hamiltonian $H(t)$ by $|\varepsilon_j(t)\rangle$ where $\varepsilon_j(t)$ marks the j -th energy level, $j \in \mathbb{N}_0$. We may write:

$$H(t)|\varepsilon_j(t)\rangle = \varepsilon_j(t)|\varepsilon_j(t)\rangle. \quad (13)$$

It is usually convenient to introduce a particular labeling of the eigenvalues. While examining time-dependent Hamiltonians, we may label the eigenvalues using the ordering: $j < k \implies \varepsilon_j(t) \leq \varepsilon_k(t)$. Having initialized the system subjected to the time dependent Hamiltonian $H(t)$ the labeling helps us to discern between different eigenvalues and enables us to track their evolution. If we begin in an eigenstate $|\varepsilon_j(0)\rangle$, the evolved state will follow the path ³ of instantaneous eigenstates $|\varepsilon_j(t)\rangle$ for all times $t \in [0, T]$, where T denotes the total time of the evolution, provided that [30]

$$\max_{t \in [0, T]} \frac{|\langle \varepsilon_i | \partial_t \varepsilon_j \rangle|}{|\varepsilon_i - \varepsilon_j|} = \max_{t \in [0, T]} \frac{|\langle \varepsilon_i | \partial_t H | \varepsilon_j \rangle|}{|\varepsilon_i - \varepsilon_j|^2} \ll 1 \quad \forall i \neq j. \quad (14)$$

In 2009, Amin found a way to improve the assumptions (14) so that the AT holds generally [29]. He pointed out that using a suitable reparametrisation of the time scale leads to a criterion providing a variant of AT analogous to the Messiah’s (14) [30]. Let s be from the interval $[0, 1]$. We may see that the Schrödinger equation can be rewritten using $s = \frac{t}{T}$ as follows

$$\frac{i}{T} \frac{\partial |\tilde{\psi}(s)\rangle}{\partial s} = \tilde{H}(s) |\tilde{\psi}(s)\rangle, \quad (15)$$

where $\tilde{H}(s) = H(sT)$ and $|\tilde{\psi}(s)\rangle = |\psi(sT)\rangle$. The variable s is called dimensionless time and we will further omit tildes while expressing dependency on it.

The adiabatic theorem holds provided that the $H(s)$ parameterized by the dimensionless time s does not explicitly depend on T and if

$$\max_{s \in [0, 1]} \frac{|\langle \varepsilon_i(s) | \partial_s H(s) | \varepsilon_j(s) \rangle|}{|\varepsilon_i(s) - \varepsilon_j(s)|^2} \ll T \quad \forall j \neq i. \quad (16)$$

²Also known as *classical*. This name, however, does not imply any direct connection to the *classical physics*. The term *classical* means “first known”.

³Up to global phase factor.

For the interpolating Hamiltonians of the form

$$H(s) = sH_0 + (1 - s)H_1, \quad (17)$$

suitable for the AQC, we are usually able to guarantee the above conditions if the time scale s grows monotonically and provided that the final Hamiltonian H_1 does not depend on the runtime T ⁴.

Recall the adiabatic condition (16); if the operator $\partial_s H$ is bounded⁵ we may set $B(s) = \|\partial_s H\|$. Then we arrive at a useful bound for the total runtime T , $\forall j \neq i$:

$$\max_{s \in [0,1]} \frac{|\langle \varepsilon_i(s) | \partial_s H(s) | \varepsilon_j(s) \rangle|}{|\varepsilon_i(s) - \varepsilon_j(s)|^2} < \max_{s \in [0,1]} \frac{|\langle \varepsilon_i(s) | B(s) | \varepsilon_j(s) \rangle|}{|\varepsilon_i(s) - \varepsilon_j(s)|^2} \quad (18)$$

$$< \max_{s \in [0,1]} \frac{B(s)}{|\varepsilon_i(s) - \varepsilon_j(s)|^2} \quad (19)$$

$$= \max_{s \in [0,1]} \frac{B(s)}{\varepsilon_{ij}(s)^2} \ll T, \quad (20)$$

where $\varepsilon_{ij}(s)$ stands for $|\varepsilon_i(s) - \varepsilon_j(s)|$. An (ij) -th spectral gap may be defined as

$$\Delta_{ij} = \min_{s \in [0,1]} \varepsilon_{ij}(s). \quad (21)$$

With the use of (21) the equation (18) can be further estimated as follows:

$$\max_{s \in [0,1]} \frac{B(s)}{\varepsilon_{ij}(s)^2} < \max_{s \in [0,1]} \frac{B(s)}{\Delta_{ij}^2}. \quad (22)$$

An estimate on the operator $\partial_s H$ was used together with the fact that T is significantly greater than the left-hand side (18). An inverse-square dependence may be seen in (18) and (22); from here arise names for such bounds: “inverse square spectral gap” etc [14].

Various more precise bounds may be found; they are usually of the form $O(\frac{1}{T^n})$ for $n \in \mathbb{N}$ [31] or [32]. We will not present a proof of any of the refined alternatives as (18) and (22) suffices for our purposes. For a deeper analysis and alternative statements of the inverse spectral gap rule see, for example [32].

We will conclude this section by adding two remarks [36]: one concerning a structural aspect of the proof, second regarding a possibility of achieving an arbitrarily small error in the resulting state.

1. While introducing the adiabatic theorem, a note regarding a phase factor was added. We shall return to the discussion of the phase evolution in the following paragraphs. Let $H(s)$ be a Hamiltonian⁶ with an eigenvector $\psi(s)$. Physically, for any parameter κ , a vector $|\phi(s)\rangle$ defined as $|\phi(s)\rangle = e^{i\kappa s}|\psi(s)\rangle$ is an equally suitable eigenvector, the phase factor is not of observable significance. One may easily see that unless $\kappa = 0$ it is not possible to make $\psi(s)$ and $\phi(s)$ arbitrarily close in norm. This may cause problems while making statements about closeness of evolved states. Several solutions are available.

⁴When it does, additional investigation has to be performed.

⁵Up until now we have been implicitly presuming existence of required derivatives and in cases where operators have been derivated also boundedness of their derivatives.

⁶ $H(s)$ is considered to be a reparametrization of a Hamiltonian $H(t)$ that uses dimensionless time.

One approach is based on replacing of the objects to be investigated – vectors with physically insignificant global phase – to objects without such an attribute – for example, rays or projectors. Then the adiabatic theorem becomes a statement about evolution of projectors onto eigenspaces. This idea appeared for the first time in Kato’s proof [26] and was later studied by various authors: for instance [33] and [34].

Another approach is based on elimination of the rotational phase factor. A suitable selection of complex factors was investigated in [31]. We will only point a Lemma from [31] enabling us to regard evolution of eigenvectors:

Lemma 1.1. *Let $\psi(s)$, $0 \leq s \leq 1$, be a time-dependent unit vector in some Hilbert space H , such that $\psi(s)$ is a differentiable function of s . Then, there is another time-dependent unit vector $\phi(s)$ that is identical to $\psi(s)$ up to phase such that $\frac{d}{ds}\langle\phi(s)|\phi(s)\rangle = 0$ and $\phi(0) = \psi(0)$.*

Provided we are able to fulfill conditions outlined in the Lemma 1.1 we may track evolution of the eigenstates directly [31].

2. In the criteria (18) and (22) we imposed rather imprecise conditions on the total runtime T : we were only advised to pick T a lot greater than something. Is there any way how to make the estimate how precise the resulting state is?

These questions were investigated in Nenciu’s work [33] and later in [35]. We will not go through the derivation of statements presented in the latter articles nor will we state them precisely as they are rather complicated and some theoretical background is needed [36].

The major result of [35] will be summarized in the following lines. Assume for simplicity that we investigate conditions for the two lowest eigenvalues and suppose further that $\varepsilon_0(s) = 0$, i.e. the eigenvalue corresponding to the ground state is zero during the evolution. Let the phase be fixed as in the Lemma 1.1: $\frac{d}{ds}\langle\varepsilon_0(s)|\varepsilon_0(s)\rangle = 0$. Under these conditions the following theorem holds [35] [14]:

Theorem 1.2. *Assume that all derivatives of the Hamiltonian $H(s)$ vanish at $s \in \{0, 1\}$, and moreover that it satisfies the following condition: there exist constants $C, R, \alpha > 0$ such that for all $k \geq 1$,*

$$\max_{s \in [0,1]} \|H^{(k)}(s)\| \leq CR^k \frac{(k!)^{1+\alpha}}{(k+1)^2}. \quad (23)$$

Then the adiabatic error is bounded as

$$\min_{\theta} \|\psi(1) - e^{i\theta}|\varepsilon_0(1)\rangle\| \leq c_1 \frac{C}{\Delta} \exp\left(\left(-\frac{c_2 \Delta^3 T}{C^2}\right)^{1/(1+\alpha)}\right), \quad (24)$$

where $c_1 = eR(8\pi^2/3)$ and $c_2 = \frac{3/4\pi^2}{4eR^2}$.

Thus, as long as $T \gg \frac{C^2}{\Delta^3}$ and as long as the conditions of the theorem 1.2 holds and with latter prerequisites, the adiabatic error is exponentially small in T [14].

Further comments on the estimates of error is available in [14].

2 The Hadamard walk

The Hadamard walk is a standard model for a discrete time quantum walk [37]. Suppose the walker is located on an infinite discretized line – the position space

$$\mathcal{H}_n = \text{span}\{|i\rangle | i \in \mathbb{Z}\}. \quad (25)$$

In the previous chapter, we introduced conditional shifts on a continuous line using the equation (8). Instead of using $|\psi(x_0)\rangle$ to denote a particle at a point x_0 we shall use $|x_0\rangle$. In this discrete model we will no longer allow the shift l to take any value: from now on we fix $l = 1$. In order to enable conditional shifts, we augment the position space with a so-called coin space \mathcal{H}_c in analogy to the spin space for spin- $\frac{1}{2}$ particles from the previous section. We keep the notation and say that \mathcal{H}_c is spanned by vectors $|\downarrow\rangle, |\uparrow\rangle$. The evolution is then taking place in $\mathcal{H}_c \otimes \mathcal{H}_n$ and it is again governed by a conditional shift operator analogous to (9):

$$S = |\downarrow\rangle\langle\downarrow| \otimes \sum_n |i-1\rangle\langle i| + |\uparrow\rangle\langle\uparrow| \otimes \sum_n |i+1\rangle\langle i|. \quad (26)$$

This choice implies that $S|\uparrow\rangle|p\rangle = |\uparrow\rangle|p+1\rangle$ and $S|\downarrow\rangle|p\rangle = |\downarrow\rangle|p-1\rangle$; the up/down notation $|\downarrow\rangle, |\uparrow\rangle$ agrees with the direction of the conditional shift. The random walk is realised as a two step process:

1. We perform a unitary operation C in the coin space called *tossing a coin*.
2. The conditional shift S from the equation (26) is applied.

Usually, steps 1 and 2 are thought of as a single iteration of the random walk. By a suitable choice of the coin operation C , we may mimic a classical walk. Starting with the state $|\downarrow\rangle|0\rangle$, we expect to measure the position of the walker ± 1 after a single iteration. The unitary coin should map $|\downarrow\rangle$ to a uniform superposition of $|\downarrow\rangle$ and $|\uparrow\rangle$ and similarly for $|\uparrow\rangle$. The conventional choice of the balanced coin operator is [1]

$$C = H = \begin{pmatrix} s & s \\ s & -s \end{pmatrix}, \quad (27)$$

where $s = \frac{1}{\sqrt{2}}$, equal to the Hadamard gate (11), giving name to the Hadamard walk.

The evolution governed by the successive application of C and S may be written as:

$$U = S(C \otimes I) = \left(|\downarrow\rangle\langle\downarrow| \otimes \sum_n |i-1\rangle\langle i| + |\uparrow\rangle\langle\uparrow| \otimes \sum_n |i+1\rangle\langle i| \right) (C \otimes I). \quad (28)$$

In this case we apply the same unitary operation C at all positions of the grid \mathbb{Z} .

While studying quantum random walks we are not primarily interested in simulating classical walks but we let the walker evolve without the intermediate measurements. Without resetting the internal spin, quantum walks differ significantly from classical. We adopt an illustrative example from [1]. Beginning in the state $|\uparrow\rangle \otimes |0\rangle$ we shall proceed a few steps of the evolution:

$$\begin{aligned} \text{step 0} & \quad |\uparrow\rangle \otimes |0\rangle, \\ \text{step 1} & \quad s(|\downarrow\rangle \otimes |-1\rangle - |\uparrow\rangle \otimes |1\rangle), \\ \text{step 2} & \quad \frac{1}{2}(|\downarrow\rangle \otimes |-2\rangle + (|\downarrow\rangle - |\uparrow\rangle) \otimes |0\rangle + |\uparrow\rangle \otimes |2\rangle), \\ \text{step 3} & \quad \frac{s}{2}(|\downarrow\rangle \otimes |-3\rangle + |\uparrow\rangle \otimes |-1\rangle + |\downarrow\rangle \otimes |1\rangle - 2|\uparrow\rangle \otimes |1\rangle - |\uparrow\rangle \otimes |3\rangle). \end{aligned} \quad (29)$$

The resulting probability distribution differs from that of classical walks even after such small number of steps. It is convenient to introduce coordinates on $\mathbb{C}^2 \otimes \text{span}\{|n\rangle\}$ with basis $\{|\downarrow\rangle \otimes |n\rangle, |\uparrow\rangle \otimes |n\rangle\}$. For this case we use column vectors $\begin{pmatrix} \alpha_n \\ \beta_n \end{pmatrix}$. In order to describe a point in $\mathbb{C}^{2\mathbb{Z}}$ we use a pair of sequences $(\alpha_n)_{n \in \mathbb{Z}}$ and $(\beta_n)_{n \in \mathbb{Z}}$ with the normalizing condition:

$$\sum_{n \in \mathbb{Z}} \left\| \begin{pmatrix} \alpha_n \\ \beta_n \end{pmatrix} \right\|^2 = 1. \quad (30)$$

We note that the probability of $p(n)$ finding a walker at a node n equals

$$p(n) = \left\| \begin{pmatrix} \alpha_n \\ \beta_n \end{pmatrix} \right\|^2. \quad (31)$$

Returning to the equation (29) we see that the resulting probability distribution is not symmetric. Furthermore, it clearly depends on the way we set the initial state up. The problem of determining initial states leading to symmetrical distributions has been investigated [38]. The choice of the initial state we used in our simulations is:

$$\psi_0 = s(|\uparrow\rangle + i|\downarrow\rangle) \otimes |0\rangle. \quad (32)$$

We will not perform step-by-step iteration as in the equation (29) to deduce symmetry. The Hadamard coin has only real elements, so that it does not introduce any imaginary amplitudes when we initialize the walk with only real α 's and β 's. But analogous property holds for only imaginary α 's and β 's. Having thus initialised the Hadamard walk in the state ψ_0 (32) and taking into account (31) we find the resulting probability distribution will be symmetrical. In Figure 2 the resulting probability distribution after having performed 30 steps of the Hadamard walk is plotted. We did not center the walk around zero but rather around the 75th node.

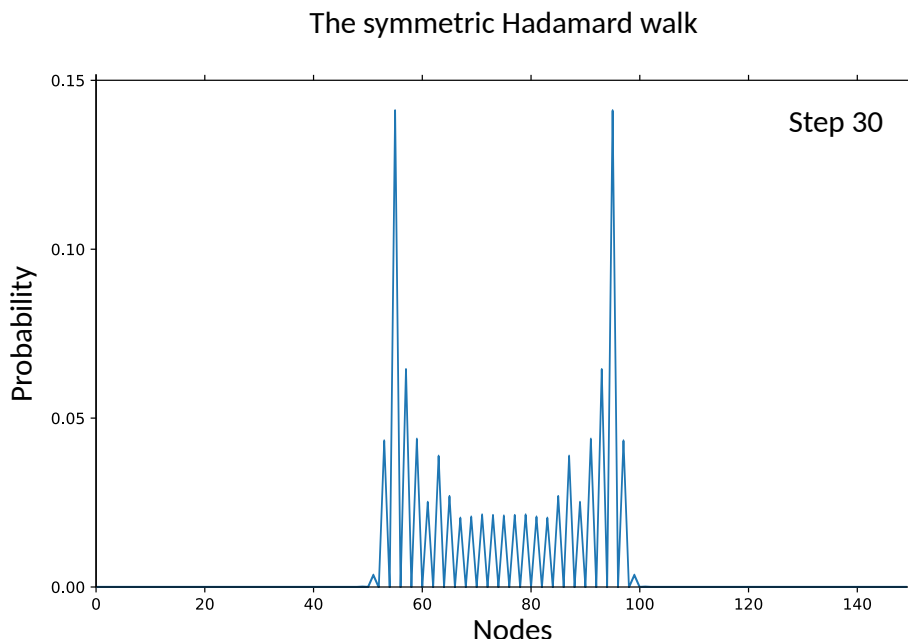


Figure 2: The resulting probability distribution of the Hadamard walk with the initial setting corresponding to (32) (shifted to the node 75).

2.1 Finite-dimensional case and additional boundary conditions

In the following sections, we will discuss adiabatic transitions of the underlying coin space operators in the equation (28). These transitions will require finding paths in unitary groups $U(n)$, which leads to numerically complicated computations. In order to simplify our task we used numerical simulations of these transitions. Even though computers are increasingly more powerful, they are principally incapable of storing the whole state space of a quantum random walk. Modern programming offers solutions and enables us to perform clever tricks [39]. A different approach is to restrict the state space of the quantum walk to a finite lattice. Then we may benefit from known and fixed dimensions of the state space and actually perform our computations faster. This approach carries an inherent drawback: it is necessary to construct a finite model of the investigated system and introduce new boundary conditions that arise on previously non-existent bounds.

Beginning with the equation (28), we examine the evolution on a finite grid containing, say, N points. We will try to preserve evolution (28) at the internal points and then derive necessary conditions we have to add in order to guarantee unitarity of the evolution. The underlying Hilbert space governing the finite dimensional case is $\mathbb{C}^2 \otimes \text{span}\{|0\rangle, |1\rangle, \dots, |N-1\rangle\} \simeq \mathbb{C}^{2N}$. We shall use coordinatization of $\mathbb{C}^2 \otimes \text{span}\{|n\rangle\}$ with basis $\{|\downarrow\rangle \otimes |n\rangle, |\uparrow\rangle \otimes |n\rangle\}$ using column vector $\begin{pmatrix} \alpha_n \\ \beta_n \end{pmatrix}$ and will form a large column vector describing a point in \mathbb{C}^{2N} :

$$x \in \mathbb{C}^{2N} \mapsto ((\alpha_0(x), \beta_0(x)), (\alpha_1(x), \beta_1(x)), \dots, (\alpha_{N-1}(x), \beta_{N-1}(x)))^T, \quad (33)$$

where v^T denotes the transpose of v . The evolution operator (28) combines the conditional shift (26) together with tossing of the coin. The conditional shift at position $n \in \{0, 1, \dots, N-1\} = \widehat{N-1}$ enables the walker to move one step left or right depending on the internal state $\begin{pmatrix} \alpha_n \\ \beta_n \end{pmatrix} \in \mathbb{C}^2 \otimes \text{span}\{|n\rangle\}$. In this sense the evolution acts *locally*: amplitudes $\alpha_n(t), \beta_n(t)$ at a step t depend only on those at near neighbourhood at the previous time step. We thus modify the evolution matrix only at rows corresponding to $\begin{pmatrix} \alpha_0 \\ \beta_0 \end{pmatrix}$ and $\begin{pmatrix} \alpha_{N-1} \\ \beta_{N-1} \end{pmatrix}$. Such choice thus frees the first and last nodes to some extent and enables us to change the definition of *locality* for them. For $n \in \{1, 2, \dots, N-2\}$ the evolution (28) maps $\begin{pmatrix} \alpha_n(t) \\ \beta_n(t) \end{pmatrix} \otimes |n\rangle$ at time t to $s(\alpha_n(t) + \beta_n(t))|\downarrow\rangle|n-1\rangle + s(\alpha_n(t) - \beta_n(t))|\uparrow\rangle|n+1\rangle$. Thus:

$$\begin{aligned} \alpha_{n-1}(t+1) &= s(\alpha_n(t) + \beta_n(t)), \\ \beta_{n+1}(t+1) &= s(\alpha_n(t) - \beta_n(t)). \end{aligned} \quad (34)$$

We shall find a way to change the evolution of $\begin{pmatrix} \alpha_0 \\ \beta_0 \end{pmatrix}$ and $\begin{pmatrix} \alpha_{N-1} \\ \beta_{N-1} \end{pmatrix}$ in order to preserve unitarity of the evolution operator. The evolution operator will be written in a matrix form and we will expand the set of equations (34) by four rows governing the evolution

at locations 0 and $N - 1$:

$$U = \begin{pmatrix} a_1 & a_2 & a_3 & a_4 & a_5 & a_6 & a_7 & a_8 & \dots & a_{N-4} & a_{N-3} & a_{N-2} & a_{N-1} \\ b_1 & b_2 & b_3 & b_4 & b_5 & b_6 & b_7 & b_8 & \dots & b_{N-4} & b_{N-3} & b_{N-2} & b_{N-1} \\ 0 & 0 & 0 & 0 & s & s & 0 & 0 & \dots & 0 & 0 & 0 & 0 \\ s & -s & 0 & 0 & 0 & 0 & 0 & 0 & \dots & 0 & 0 & 0 & 0 \\ 0 & 0 & 0 & 0 & 0 & 0 & s & s & \dots & 0 & 0 & 0 & 0 \\ 0 & 0 & s & -s & 0 & 0 & 0 & 0 & \dots & 0 & 0 & 0 & 0 \\ 0 & 0 & 0 & 0 & 0 & 0 & 0 & 0 & \dots & 0 & 0 & 0 & 0 \\ 0 & 0 & 0 & 0 & s & -s & 0 & 0 & \dots & 0 & 0 & 0 & 0 \\ \vdots & \ddots & \vdots & \vdots & \vdots & \vdots \\ 0 & 0 & 0 & 0 & 0 & 0 & 0 & 0 & \dots & 0 & 0 & s & s \\ 0 & 0 & 0 & 0 & 0 & 0 & 0 & 0 & \dots & 0 & 0 & 0 & 0 \\ c_1 & c_2 & c_3 & c_4 & c_5 & c_6 & c_7 & c_8 & \dots & c_{N-4} & c_{N-3} & c_{N-2} & c_{N-1} \\ d_1 & d_2 & d_3 & d_4 & d_5 & d_6 & d_7 & d_8 & \dots & d_{N-4} & d_{N-3} & d_{N-2} & d_{N-1} \end{pmatrix}. \quad (35)$$

The four highlighted elements illustrate distribution of the elements of the Hadamard coin at an inner node $n = 2$ in the evolution matrix. Because we chose the position 2, we find the original elements in the $(2 \cdot (n + 1))$ -th column at rows $(2 \cdot (n + 1)) - 3$ and $(2 \cdot (n + 1)) + 2$. The unitarity of U will impose additional conditions on vectors $\vec{a}, \vec{b}, \vec{c}, \vec{d}$:

$$UU^\dagger \stackrel{!}{=} I, \quad (36)$$

where \dagger denotes a Hermitian transpose. Performing the calculation (36) we find the additional conditions:

$$a_1 - a_2 = a_3 - a_4 = a_{N-4} + a_{N-3} = a_{N-2} + a_{N-1} = 0, \quad (37)$$

$$b_1 - b_2 = b_3 - b_4 = b_{N-4} + b_{N-3} = b_{N-2} + b_{N-1} = 0, \quad (38)$$

$$c_1 - c_2 = c_3 - c_4 = c_{N-4} + c_{N-3} = c_{N-2} + c_{N-1} = 0, \quad (39)$$

$$d_1 - d_2 = d_3 - d_4 = d_{N-4} + d_{N-3} = d_{N-2} + d_{N-1} = 0, \quad (40)$$

$$(\forall i \in \{5, 6, \dots, N - 6, N - 5\}) (a_i = b_i = c_i = d_i = 0) \quad (41)$$

and

$$\langle a|b \rangle = \langle a|c \rangle = \langle a|d \rangle = 0, \quad (42)$$

$$\langle b|c \rangle = \langle b|d \rangle = \langle c|d \rangle = 0, \quad (43)$$

$$\langle a|a \rangle = \langle b|b \rangle = 1, \quad (44)$$

$$\langle d|d \rangle = \langle c|c \rangle = 1. \quad (45)$$

One particularly intuitive solution to the equations (37) to (45) may be obtained by twisting the grid $\{0, 1, \dots, N - 1\}$, so that the point 0 becomes a right neighbour of $N - 1$ an vice versa. The solution may be written explicitly:

$$\begin{aligned} a_3 &= s, & a_4 &= s, \\ b_{N-2} &= s, & b_{N-1} &= -s, \\ c_1 &= s, & c_2 &= s, \\ d_{N-4} &= s, & d_{N-3} &= -s, \end{aligned} \quad (46)$$

and all non-listed elements of the vectors a, b, c, d are zero. This choice of boundary condition will be called periodic boundary condition and we performed most of numerical simulations in this setting.

Note that the periodic boundary is equivalent to considering positions as points of $\mathbb{Z}_N = \mathbb{Z}/N\mathbb{Z}$.

2.2 Analysis of coin-space defects

A quantum walker on an infinite line will undergo a discrete evolution that may be described as a sequence of two operations: at first a coin is tossed and then the shift operator shifts the walker accordingly. A straightforward generalisation of the equation (28) leads us to coin space transformations dependent on the position:

$$U = S \left(\bigoplus_{n \in \mathbb{Z}} C_n \right), \quad (47)$$

where

$$S = |\downarrow\rangle\langle\downarrow| \otimes \sum_{n \in \mathbb{Z}} |n-1\rangle\langle n| + |\uparrow\rangle\langle\uparrow| \otimes \sum_{n \in \mathbb{Z}} |n-1\rangle\langle n|, \quad (48)$$

and $\forall n \in \mathbb{Z}$ C_n is a unitary transform [40]. We shall examine eigenvalues of a Hadamard walk with one defect located at point $x = 0$. Let the coin defect be

$$C_0 = \begin{pmatrix} x_{11} & x_{12} \\ x_{21} & x_{22} \end{pmatrix}, \quad (49)$$

where $x_{11}, x_{12}, x_{21}, x_{22} \in \mathbb{C}$ and $C_0 \cdot C_0^\dagger = I$, and for all $n \in \mathbb{Z} \setminus \{0\}$, $C_n = H$. Note that we may set the position of the defect to $n = 0$ without loss of generality.

Suppose there is an eigenvector

$$|\psi\rangle = \sum_{n \in \mathbb{Z}} (\alpha_n |\downarrow\rangle + \beta_n |\uparrow\rangle) \otimes |n\rangle \quad (50)$$

with a corresponding eigenvalue λ . Performing a step of the evolution from time t to $t + 1$ we obtain:

$$\begin{aligned} |\psi(t+1)\rangle &= U|\psi(t)\rangle = \sum_{n \in \mathbb{Z}} (\alpha_n(t+1) |\downarrow\rangle + \beta_n(t+1) |\uparrow\rangle) \otimes |n\rangle \\ &= (x_{11}\alpha_0(t) + x_{12}\beta_0(t)) |\downarrow\rangle \otimes |-1\rangle + (x_{21}\alpha_0(t) + x_{22}\beta_0(t)) |\uparrow\rangle \otimes |1\rangle \\ &\quad + \sum_{n \in \mathbb{Z} \setminus \{0\}} (s\alpha_n(t) + s\beta_n(t)) |\downarrow\rangle \otimes |n-1\rangle \\ &\quad + \sum_{n \in \mathbb{Z} \setminus \{0\}} (s\alpha_n(t) - s\beta_n(t)) |\uparrow\rangle \otimes |n+1\rangle \\ &\stackrel{!}{=} \lambda \sum_{n \in \mathbb{Z}} (\alpha_n(t) |\downarrow\rangle + \beta_n(t) |\uparrow\rangle) \otimes |n\rangle. \end{aligned} \quad (51)$$

Having collected corresponding coefficients from both sides of (51), we are led to the following set of equations:

$$\begin{aligned} x_{11}\alpha_0(t) + x_{12}\beta_0(t) &= \lambda\alpha_{-1}(t) = \alpha_{-1}(t+1), \\ x_{21}\alpha_0(t) + x_{22}\beta_0(t) &= \lambda\beta_1(t) = \beta_1(t+1), \end{aligned} \quad (52)$$

$$\begin{aligned}\forall n \in \mathbb{Z} \setminus \{-1\} \quad s(\alpha_{n+1}(t) + \beta_{n+1}(t)) &= \lambda \alpha_n(t) = \alpha_n(t+1), \\ \forall n \in \mathbb{Z} \setminus \{1\} \quad s(\alpha_{n-1}(t) - \beta_{n-1}(t)) &= \lambda \beta_n(t) = \beta_n(t+1).\end{aligned}\tag{53}$$

Our aim is to find sequences $(\alpha_n)_{n \in \mathbb{Z}}, (\beta_n)_{n \in \mathbb{Z}}$ together with the corresponding eigenvalue λ . Before presenting our attempt to solve the eigenvalue problem concerning Hadamard walks with coin defects, we shall briefly outline two cases already studied, namely phase-altered coin defect and a coin defect with rotation matrix. These perturbations will be revisited in our formalism as examples.

2.2.1 Known cases

The eigenvalue problem (51) has been investigated in several cases. We will briefly comment on coin defects introduced by Wójcik et al. [2]. They considered a coin perturbation of the form:

$$C_0 = \exp(2\pi i \phi) \cdot \begin{pmatrix} s & s \\ s & -s \end{pmatrix} = \omega \cdot H.\tag{54}$$

Rather than solving the set of difference equations (52), (53) directly Wójcik et al. opted for analyzing an eigenvalue problem for a two-step evolution. This leads to a system of two-step difference equations:

$$\begin{aligned}2\lambda \tilde{\alpha}_0 &= \tilde{\alpha}_1 + \tilde{\beta}_1 + \omega \tilde{\alpha}_0 - \omega \tilde{\beta}_0, \\ 2\lambda \tilde{\beta}_0 &= \omega \tilde{\alpha}_0 - \omega \tilde{\beta}_0 - \tilde{\alpha}_{-1} + \tilde{\beta}_{-1}, \\ 2\lambda \tilde{\alpha}_{-1} &= \omega \tilde{\alpha}_0 + \omega \tilde{\beta}_0 + \tilde{\alpha}_{-1} - \tilde{\beta}_{-1}, \\ 2\lambda \tilde{\beta}_1 &= \tilde{\alpha}_1 + \tilde{\beta}_1 - \omega \tilde{\alpha}_0 + \omega \tilde{\beta}_{-1},\end{aligned}\tag{55}$$

for the neighbourhood of $\tilde{\alpha}_0, \tilde{\beta}_0$, where:

$$\tilde{\alpha}_n = \alpha_{2n},\tag{56}$$

$$\tilde{\beta}_n = \beta_{2n},\tag{57}$$

and

$$\begin{aligned}2\lambda \tilde{\alpha}_n &= \tilde{\alpha}_{n+1} + \tilde{\beta}_{n+1} + \tilde{\alpha}_n - \tilde{\beta}_n \quad \text{for } n \neq 0, -1, \\ 2\lambda \tilde{\beta}_n &= \tilde{\alpha}_n + \tilde{\beta}_n - \tilde{\alpha}_{n-1} + \tilde{\beta}_{n-1} \quad \text{for } n \neq 0, 1.\end{aligned}\tag{58}$$

Wójcik et al. found the solutions for λ to be:

$$\lambda_{\pm} = \frac{\omega - 2\omega^2 + \omega^3 \pm i\omega(1 - \omega + \omega^2)}{1 - 2\omega + 2\omega^2}.\tag{59}$$

The above equation yields stationary states:

$$\begin{aligned}\tilde{\alpha}_n^{\pm} &= C x_{\pm}^n \quad \text{for } n \geq 1, \\ \tilde{\alpha}_n^{\pm} &= C(\omega \mp i\omega \pm i)x_{\pm}^{-n} \quad \text{for } n \leq -1\end{aligned}\tag{60}$$

and for $\tilde{\beta}$

$$\begin{aligned}\tilde{\beta}_n^{\pm} &= C(1 - \omega \mp i\omega)x_{\pm}^n \quad \text{for } n \geq 1, \\ \tilde{\beta}_n^{\pm} &= \mp i C x_{\pm}^{-n} \quad \text{for } n \leq -1,\end{aligned}\tag{61}$$

where

$$x_{\pm} = \frac{1}{2 \cos(\omega) \mp 2 \sin(\omega) - 3}. \quad (62)$$

Finally, explicit formulas for $\tilde{\alpha}_0, \tilde{\beta}_0$ were derived:

$$\tilde{\alpha}_0^{\pm} = C, \tilde{\beta}_0^{\pm} = \mp iC. \quad (63)$$

The constant C plays a role of normalizing constant and it may be chosen as:

$$C = \sqrt{\frac{1 + x_{\pm}}{2}}. \quad (64)$$

Another type of coin defect was studied by Endo and Konno in [40]. They introduced a single perturbation:

$$C_0 = \begin{pmatrix} \cos(\theta) & \sin(\theta) \\ \sin(\theta) & -\cos(\theta) \end{pmatrix} \quad (65)$$

at the origin of an infinite discrete line. In contrast to the Wójcik model with phase-altered coin (54), this choice of coin defect has the property:

$$\det(C_0) = -\cos^2(\theta) - \sin^2(\theta) = \det(H) = -1. \quad (66)$$

With the intention of comparing our approach to that of Endo and Konno we will slightly adapt their notation. We are to solve an eigenvalue problem

$$U\Psi = \lambda\Psi, \quad (67)$$

for U defined in terms of the equation (48) and where

$$\Psi = (\dots, \alpha_{-1}, \beta_{-1}, \alpha_0, \beta_0, \alpha_1, \beta_1, \dots)^T. \quad (68)$$

Endo and Konno derived that the eigenvalue problem (67) may be restated as follows:

$$(\forall n \in \mathbb{Z}) : \quad \lambda \begin{pmatrix} \alpha_n \\ \beta_n \end{pmatrix} = \begin{pmatrix} a_{n+1} & b_{n+1} \\ 0 & 0 \end{pmatrix} \begin{pmatrix} \alpha_{n+1} \\ \beta_{n+1} \end{pmatrix} \begin{pmatrix} 0 & 0 \\ c_{n-1} & d_{n-1} \end{pmatrix} \begin{pmatrix} \alpha_{n-1} \\ \beta_{n-1} \end{pmatrix}, \quad (69)$$

where

$$(\forall n \in \mathbb{Z} \setminus \{0\}) : \quad \begin{pmatrix} a_n & b_n \\ c_n & d_n \end{pmatrix} = H = \begin{pmatrix} s & s \\ s & -s \end{pmatrix} \quad (70)$$

and

$$\begin{pmatrix} a_0 & b_0 \\ c_0 & d_0 \end{pmatrix} = \begin{pmatrix} \cos(\theta) & \sin(\theta) \\ \sin(\theta) & -\cos(\theta) \end{pmatrix}. \quad (71)$$

Endo and Konno used a so-called SGF method that already proved to be a viable and helpful tool to investigate eigenvalue problems concerning discrete time quantum walks [41]. In the latter article Endo and Konno revisited Wójcik model (54) and found the stationary states with the help of generating functions. We will not introduce this technique but rather address the reader to the original article [41].

Unlike in Wójcik model for which we had a pair of solutions, the problem Endo and Konno investigated admits four eigenvalues:

$$\lambda_{1,2} = \pm \frac{\cos \theta + (\sqrt{2} - \sin \theta)i}{\sqrt{3 - 2\sqrt{2} \sin \theta}}, \quad (72)$$

$$\lambda_{3,4} = \pm \frac{\cos \theta - (\sqrt{2} - \sin \theta)i}{\sqrt{3 - 2\sqrt{2} \sin \theta}}. \quad (73)$$

and their corresponding eigenvectors are of the form:

$$\begin{pmatrix} \alpha_n \\ \beta_n \end{pmatrix}_{1,2} = \begin{cases} \begin{pmatrix} \alpha_0 \\ \beta_0 \end{pmatrix} & n = 0, \quad (74) \end{cases}$$

$$\begin{cases} \left(\frac{\pm i}{\sqrt{3 - 2\sqrt{2}\sin\theta}} \right)^n \begin{pmatrix} \alpha_0 \\ \beta_0 (1 - \sqrt{2}\sin\theta)\alpha_0 + \sqrt{2}\cos\theta\beta_0 \end{pmatrix} & n \geq 1, \quad (75) \end{cases}$$

$$\begin{cases} \left(\frac{\mp i}{\sqrt{3 - 2\sqrt{2}\sin\theta}} \right)^{-n} \begin{pmatrix} \alpha_0 (\sqrt{2}\sin\theta - 1)\beta_0 + \sqrt{2}\cos\theta\alpha_0 \\ \beta_0 \end{pmatrix} & n \leq -1 \quad (76) \end{cases}$$

for $\beta_0 = -i\alpha_0$ and

$$\begin{pmatrix} \alpha_n \\ \beta_n \end{pmatrix}_{3,4} = \begin{cases} \begin{pmatrix} \alpha_0 \\ \beta_0 \end{pmatrix} & n = 0, \quad (77) \end{cases}$$

$$\begin{cases} \left(\frac{\mp i}{\sqrt{3 - 2\sqrt{2}\sin\theta}} \right)^n \begin{pmatrix} \alpha_0 \\ \beta_0 (1 - \sqrt{2}\sin\theta)\alpha_0 + \sqrt{2}\cos\theta\beta_0 \end{pmatrix} & n \geq 1, \quad (78) \end{cases}$$

$$\begin{cases} \left(\frac{\pm i}{\sqrt{3 - 2\sqrt{2}\sin\theta}} \right)^{-n} \begin{pmatrix} \alpha_0 (\sqrt{2}\sin\theta - 1)\beta_0 + \sqrt{2}\cos\theta\alpha_0 \\ \beta_0 \end{pmatrix} & n \leq -1 \quad (79) \end{cases}$$

for $\beta_0 = i\alpha_0$.

It is important to note that until now we have not considered whether the eigenvectors obtained using the SGF method are normalizable. Endo and Konno proved that the sum (30) converges if and only if $\theta \neq \frac{\pi}{4}$. Note that this particular choice of θ resets the perturbed coin to the original Hadamard coin. In the following section we shall thoroughly comment on our solution. Although we use a similar starting point as Endo and Konno did in the equation (69) our paths bifurcate soon after that.

2.3 Eigenvalue problem for general coin defects

One way to proceed is to split two sequences $(\alpha_n)_{n \in \mathbb{Z}}, (\beta_n)_{n \in \mathbb{Z}}$ into four branches: $(\alpha_{-n})_{n \in \mathbb{N}_{-1}}, (\beta_{-n})_{n \in \mathbb{N}_0}$ and $(\alpha_n)_{n \in \mathbb{N}_0}, (\beta_n)_{n \in \mathbb{N}_0}$. Since $\mathbb{N}_0 = \{0, 1, 2, \dots\}$, positive and negative branches have one common point, namely α_0 or β_0 .

We used three different methods to solve the set of equations (52) and (53). Namely:

1. We may form vectors of type $\begin{pmatrix} \alpha_n \\ \beta_n \end{pmatrix}$ and establish two shift operators S_-, S_+ acting on $\begin{pmatrix} \alpha_n \\ \beta_n \end{pmatrix}$, where n is sufficiently distant from 0, as follows: $S_- \begin{pmatrix} \alpha_n \\ \beta_n \end{pmatrix} = \begin{pmatrix} \alpha_{n-1} \\ \beta_{n-1} \end{pmatrix}$ and $S_+ \begin{pmatrix} \alpha_n \\ \beta_n \end{pmatrix} = \begin{pmatrix} \alpha_{n+1} \\ \beta_{n+1} \end{pmatrix}$. Since we must employ the boundary condition at $n = 0$, it is convenient to begin with $\begin{pmatrix} \alpha_0 \\ \beta_0 \end{pmatrix}$, apply the boundary conditions

from equation (52) to get $\begin{pmatrix} \alpha_{\pm 1} \\ \beta_{\pm 1} \end{pmatrix}$ and then generate $\begin{pmatrix} \alpha_{-n} \\ \beta_{-n} \end{pmatrix} = S_-^{n-1} \begin{pmatrix} \alpha_{-1} \\ \beta_{-1} \end{pmatrix}$ and $\begin{pmatrix} \alpha_n \\ \beta_n \end{pmatrix} = S_+^{n-1} \begin{pmatrix} \alpha_1 \\ \beta_1 \end{pmatrix}$.

Using the structure of equations (53), we may benefit from diagonalization of S_{\pm} and from analysis of the eigenvalue problem for given recurrence equations. This method will be described with thoroughly in this section.

2. We may decouple α 's and β 's in order to establish four difference equations of second order, one for negative α 's, one for positive α 's and similarly for β 's. They all have to satisfy the boundary condition specified in equation (52) at $n = 0$. We will not present this method here because it tends to be more complicated than the latter one.
3. A numerical simulation of the Hadamard walk with a single point defect might provide us with explicit solutions of the eigenvalue problem. We will discuss the relevance of numerical simulations in the Section 3.1 and we will compare numerical and analytical solutions in relevant cases.

We shall first derive explicit formulas for operators S_{\pm} acting on an unperturbed Hadamard walk; later, a defective coin will be introduced and a more elaborate discussion regarding effects of the three boundary terms $\begin{pmatrix} \alpha_{\pm 1} \\ \beta_{\pm 1} \end{pmatrix}$ and $\begin{pmatrix} \alpha_0 \\ \beta_0 \end{pmatrix}$ will be provided.

Beginning with S_- , we search for a formula deriving $\begin{pmatrix} \alpha_{n-1} \\ \beta_{n-1} \end{pmatrix}$ from $\begin{pmatrix} \alpha_n \\ \beta_n \end{pmatrix}$. With the knowledge from equations (51) and (53) we have:

$$\alpha_{n-1} = s\lambda^{-1}(\alpha_n + \beta_n) \quad (80)$$

$$\beta_{n+1} = s\lambda^{-1}(\alpha_n - \beta_n), \quad (81)$$

where $s = \frac{1}{\sqrt{2}}$. Shifting $n \mapsto n - 1$ in equation (81), we are led to

$$\beta_n = s\lambda^{-1}(\alpha_{n-1} - \beta_{n-1}). \quad (82)$$

Thus $\begin{pmatrix} \alpha_{n-1} \\ \beta_{n-1} \end{pmatrix}$ may be expressed solely by using $\begin{pmatrix} \alpha_n \\ \beta_n \end{pmatrix}$ as follows:

$$\alpha_{n-1} = s\lambda^{-1}(\alpha_n + \beta_n) \quad (83)$$

$$\beta_{n-1} = s\lambda^{-1}(\alpha_n + (s\lambda^{-1} - s^{-1}\lambda)\beta_n), \quad (84)$$

or in a matrix form:

$$\begin{pmatrix} \alpha_{n-1} \\ \beta_{n-1} \end{pmatrix} = \underbrace{\begin{pmatrix} s\lambda^{-1} & s\lambda^{-1} \\ s\lambda^{-1} & s\lambda^{-1} - \lambda s^{-1} \end{pmatrix}}_{S_-} \begin{pmatrix} \alpha_n \\ \beta_n \end{pmatrix}. \quad (85)$$

Similar steps will provide us with a formula for S_+ . Firstly, we shift $n \mapsto n + 1$ in equation (80) and then express α_{n+1} in terms of α_n and β_{n+1} :

$$\alpha_{n+1} = s^{-1}\lambda\alpha_n - \beta_{n+1} + 1. \quad (86)$$

With the aid of the equation (81) we may write:

$$\alpha_{n+1} = (s^{-1}\lambda - s\lambda^{-1})\alpha_n + s\lambda^{-1}\beta_n \quad (87)$$

$$\beta_{n+1} = s\lambda^{-1}(\alpha_n - \beta_n), \quad (88)$$

or equivalently:

$$\begin{pmatrix} \alpha_{n+1} \\ \beta_{n+1} \end{pmatrix} = \underbrace{\begin{pmatrix} s^{-1}\lambda - s\lambda^{-1} & s\lambda^{-1} \\ s\lambda^{-1} & -s\lambda^{-1} \end{pmatrix}}_{S_+} \begin{pmatrix} \alpha_n \\ \beta_n \end{pmatrix}. \quad (89)$$

The operators S_{\pm} are in an inverse relation, indeed:

$$S_{\pm}S_{\mp} = I. \quad (90)$$

In order to solve the eigenvalue problem stated by the equation (51), we have to find a relationship between a candidate eigenvalue λ and convergence of the series

$$\sum_{n \in \mathbb{Z}} \left\| \begin{pmatrix} \alpha_n \\ \beta_n \end{pmatrix} \right\|^2. \quad (91)$$

The condition (91) encapsulates our ability to normalize the given eigenvector $\begin{pmatrix} \alpha_n \\ \beta_n \end{pmatrix}_{n \in \mathbb{Z}}$.

We shall at first examine the sequences $(\alpha_n)_{n \in \mathbb{Z}}$ and $(\beta_n)_{n \in \mathbb{Z}}$ as $n \rightarrow \pm\infty$ depending on the boundary conditions (52). Their convergence is a necessary requirement: if $(\alpha_n)_{n \in \mathbb{Z}}$ and $(\beta_n)_{n \in \mathbb{Z}}$ do not converge, the sum (91) does not converge.

The sequences $(\alpha_n)_{n \in \mathbb{Z}}$ and $(\beta_n)_{n \in \mathbb{Z}}$ encompass the solution to the recurrence equations (53).

In order to simplify required analysis, we shall diagonalize the operators S_{\pm} . Then, we will examine effect of boundary terms and branching into sequences labeled by negative and positive indices.

Since both operators S_{\pm} act on two-dimensional complex vector space, the diagonalization is straightforward, i.e.:

$$S_- = \begin{pmatrix} s\lambda^{-1} & s\lambda^{-1} \\ s\lambda^{-1} & s\lambda^{-1} - \lambda s^{-1} \end{pmatrix} = V \begin{pmatrix} \mu_1 & 0 \\ 0 & \mu_2 \end{pmatrix} V^{-1}, \quad (92)$$

where V is a matrix of eigenvectors of S_- :

$$V = \begin{pmatrix} \frac{1}{-\lambda^2 + \sqrt{\lambda^4 + 1}} & \frac{-1}{\lambda^2 + \sqrt{\lambda^4 + 1}} \\ 1 & 1 \end{pmatrix}, \quad (93)$$

$$V^{-1} = \frac{1}{\sqrt{\lambda^4 + 1}} \begin{pmatrix} \frac{1}{2} & \frac{-\lambda^2 + \sqrt{\lambda^4 + 1}}{2} \\ \frac{1}{2} & \frac{\lambda^2 + \sqrt{\lambda^4 + 1}}{2} \end{pmatrix} \quad (94)$$

and eigenvalues μ_1, μ_2 are expressed using λ as follows:

$$\begin{aligned} \mu_1 &= \frac{-\lambda^2 + 1 + \sqrt{\lambda^4 + 1}}{2\lambda s} \\ \mu_2 &= \frac{-\lambda^2 + 1 - \sqrt{\lambda^4 + 1}}{2\lambda s}. \end{aligned} \quad (95)$$

Similar relations hold for the other operator S_+ . For S_+ and S_- are inverse, they share eigenvectors. Thus:

$$S_+ = V \begin{pmatrix} \frac{1}{\mu_1} & 0 \\ 0 & \frac{1}{\mu_2} \end{pmatrix} V^{-1} \quad (96)$$

and the matrix V comes from the equation (93). There is another interesting feature operators S_{\pm} have, namely:

$$\det S_- = \mu_1 \mu_2 = -1, \quad (97)$$

$$\det S_+ = \frac{1}{\mu_1 \mu_2} = -1, \quad (98)$$

note, in particular, that determinants of S_{\pm} do not depend on λ . (We in fact had to divide by λ in order to derive (97) and (98) but we suppose λ is an eigenvalue of a unitary evolution operator so we may treat it as a nonzero number.) We will use the following relation between μ_1 and μ_2 :

$$\mu_1 = -\frac{1}{\mu_2} \quad \text{or} \quad \mu_2 = -\frac{1}{\mu_1}. \quad (99)$$

We shall now take into account the boundary conditions (52). Suppose that $\begin{pmatrix} \alpha_0 \\ \beta_0 \end{pmatrix}$ and a candidate for an eigenvalue λ are given. Using steps performed in equations (80) to (88), we find an expression for $\begin{pmatrix} \alpha_{\pm 1} \\ \beta_{\pm 1} \end{pmatrix}$ in terms of $\begin{pmatrix} \alpha_0 \\ \beta_0 \end{pmatrix}$:

$$\begin{pmatrix} \alpha_{-1} \\ \beta_{-1} \end{pmatrix} = \underbrace{\begin{pmatrix} \lambda^{-1} x_{11} & \lambda^{-1} x_{12} \\ \lambda^{-1} x_{11} & \lambda^{-1} x_{12} - \lambda s^{-1} \end{pmatrix}}_{B_-} \begin{pmatrix} \alpha_0 \\ \beta_0 \end{pmatrix}, \quad (100)$$

where x_{ij} denote the elements of the coin defect introduced in the equation (49). Having established equation (100) expressing the boundary for negative n 's, we introduce its positive counterpart:

$$\begin{pmatrix} \alpha_1 \\ \beta_1 \end{pmatrix} = \underbrace{\begin{pmatrix} \lambda s^{-1} - x_{21} \lambda^{-1} & -\lambda^{-1} x_{22} \\ \lambda^{-1} x_{21} & \lambda^{-1} x_{22} \end{pmatrix}}_{B_+} \begin{pmatrix} \alpha_0 \\ \beta_0 \end{pmatrix}. \quad (101)$$

Proposition 2.1. *If we knew $\begin{pmatrix} \alpha_0 \\ \beta_0 \end{pmatrix}$, λ and defective coin C_0 we could use the following algorithm to generate sequence $\begin{pmatrix} \alpha_n \\ \beta_n \end{pmatrix}_{n \in \mathbb{Z}}$:*

1. Derive $\begin{pmatrix} \alpha_{\pm 1} \\ \beta_{\pm 1} \end{pmatrix}$ using B_{\pm} .
2. Calculate $\begin{pmatrix} \alpha_{-n} \\ \beta_{-n} \end{pmatrix}_{n \in \mathbb{N}}$ by consecutive application of S_- on $\begin{pmatrix} \alpha_{-1} \\ \beta_{-1} \end{pmatrix}$ for any n .

3. Calculate $\begin{pmatrix} \alpha_n \\ \beta_n \end{pmatrix}_{n \in \mathbb{N}}$ by consecutive application of S_+ on $\begin{pmatrix} \alpha_1 \\ \beta_1 \end{pmatrix}$ for any n .

Furthermore, the consecutive application of S_{\pm} simplifies significantly while using equations (92) and (96). For the negative branch:

$$\begin{pmatrix} \alpha_{-n} \\ \beta_{-n} \end{pmatrix} = S_-^{n-1} B_- \begin{pmatrix} \alpha_0 \\ \beta_0 \end{pmatrix} = \left(V \begin{pmatrix} \mu_1 & 0 \\ 0 & \mu_2 \end{pmatrix} V^{-1} \right)^{n-1} B_- \begin{pmatrix} \alpha_0 \\ \beta_0 \end{pmatrix} \quad (102)$$

$$= V \begin{pmatrix} \mu_1^{n-1} & 0 \\ 0 & \mu_2^{n-1} \end{pmatrix} V^{-1} B_- \begin{pmatrix} \alpha_0 \\ \beta_0 \end{pmatrix}. \quad (103)$$

And for $n > 0$:

$$\begin{pmatrix} \alpha_n \\ \beta_n \end{pmatrix} = S_+^{n-1} B_+ \begin{pmatrix} \alpha_0 \\ \beta_0 \end{pmatrix} = \left(V \begin{pmatrix} \frac{1}{\mu_1} & 0 \\ 0 & \frac{1}{\mu_2} \end{pmatrix} V^{-1} \right)^{n-1} B_+ \begin{pmatrix} \alpha_0 \\ \beta_0 \end{pmatrix} \quad (104)$$

$$= V \begin{pmatrix} \left(\frac{1}{\mu_1}\right)^{n-1} & 0 \\ 0 & \left(\frac{1}{\mu_2}\right)^{n-1} \end{pmatrix} V^{-1} B_+ \begin{pmatrix} \alpha_0 \\ \beta_0 \end{pmatrix}. \quad (105)$$

Substituting $\mu_2 = -\frac{1}{\mu_1}$ from the equation (99):

$$\begin{pmatrix} \alpha_{-n} \\ \beta_{-n} \end{pmatrix} = V \begin{pmatrix} \mu_1^{n-1} & 0 \\ 0 & \left(-\frac{1}{\mu_1}\right)^{n-1} \end{pmatrix} \underbrace{V^{-1} B_- \begin{pmatrix} \alpha_0 \\ \beta_0 \end{pmatrix}}_{v_-}, \quad (106)$$

$$\begin{pmatrix} \alpha_n \\ \beta_n \end{pmatrix} = V \begin{pmatrix} \left(\frac{1}{\mu_1}\right)^{n-1} & 0 \\ 0 & \left(-\mu_1\right)^{n-1} \end{pmatrix} \underbrace{V^{-1} B_+ \begin{pmatrix} \alpha_0 \\ \beta_0 \end{pmatrix}}_{v_+}; \quad (107)$$

note that lower diagonal terms have $(-)$ sign.

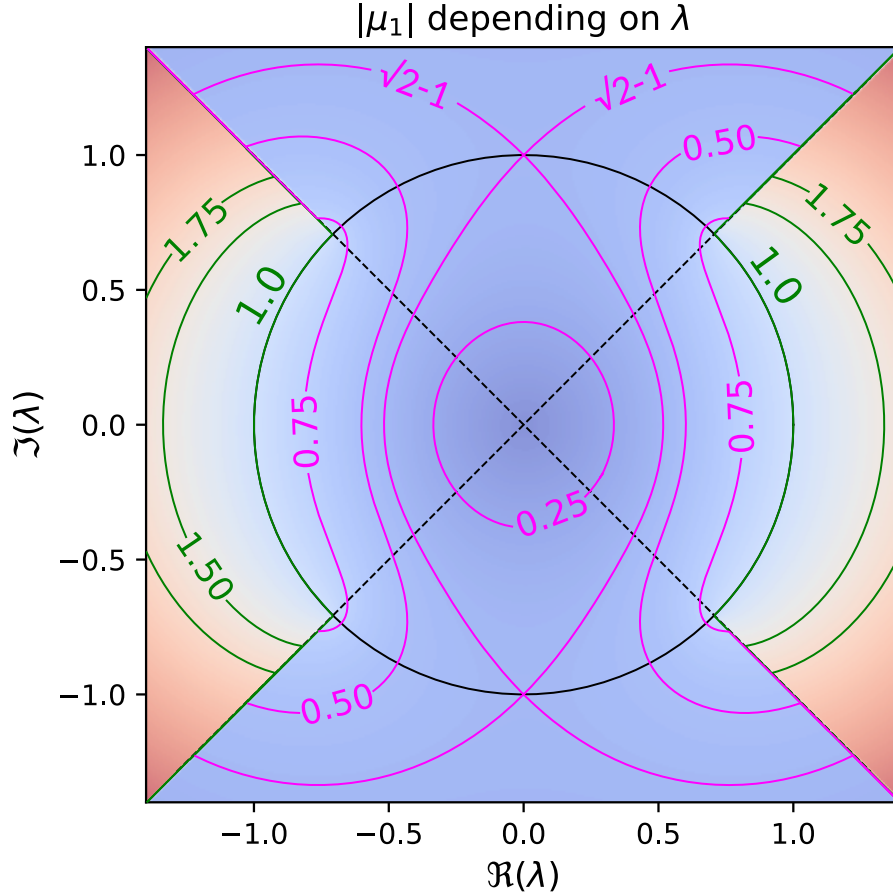


Figure 3: By plotting the absolute value $|\mu_1(\lambda)|$ in the complex plane we may uncover interesting geometric properties of solutions to be discussed. The complex plane is clearly separated to 4 regions that form a symmetric pattern. For λ is an eigenvalue of a unitary operator, $|\lambda| = 1$. We are thus interested in values of μ_1 on the unit circle. Taking into account this restriction $\mu_1 \in [\sqrt{2}-1, 1]$. We point out that $|\mu_1| = 1$ corresponds to the green contour copying parts of the unit circle. These arcs forms the continuous spectrum of the Hadamard walk. On the other hand, if $\arg(\lambda) \in (\frac{\pi}{4}, \frac{3\pi}{4}) \cup (-\frac{3\pi}{4}, -\frac{\pi}{4})$ then $|\mu_1| < 1$. (We use the convention to choose the argument of a complex number in the range $(-\pi, \pi]$.)

In order to answer the question of convergence of $\begin{pmatrix} \alpha_{\pm n} \\ \beta_{\pm n} \end{pmatrix}$ as n tends to ∞ , we have to analyze absolute values of μ_1 and μ_2 . Imagine, for example, that vector v_- has a non-zero second component and that $|\mu_1| < 1$. Then $|\frac{1}{\mu_1}| > 1$ and consecutive application of (106) will produce an unbounded sequence $(\beta_{-n})_{n \in \mathbb{N}}$.

The other three branches may produce the same type of divergent series. Similarly: if $|\mu_1| > 1$ the sequence $(\alpha_{-n})_{n \in \mathbb{N}}$ diverges unless the first component of the vector v_- vanishes.

There is another important case concerning both $|\mu_{1,2}| = 1$. Then the equations (106) and (107) imply the sum (91) will not converge unless both α_0 and β_0 are zero. Nice geometric properties of the eigenvalues $\mu_{1,2}$ of the operators S_{\pm} may be derived directly from the equation (95). A depiction of $\mu_1(\lambda)$ for the case $|\mu_1| < 1$ is shown in Figure 3.

In order to simplify notation assume (without loss of generality) that from now on the eigenvalue μ_1 has the property that $|\mu_1| < 1$. The following lemma will summarize behavior of the sequences $\begin{pmatrix} \alpha_{\pm n} \\ \beta_{\pm n} \end{pmatrix}$.

Values λ such that $|\mu(\lambda)| = 1$ form the continuous spectrum of the Hadamard walk. To be more precise $\sigma_c = \{\lambda \mid \arg(\lambda) \in [-\pi, -\frac{3\pi}{4}] \cup [-\frac{\pi}{4}, \frac{\pi}{4}] \cup [\frac{3\pi}{4}, \pi]\}$ [42].

Lemma 2.2. *Let μ and $-\frac{1}{\mu}$ be eigenvalues of the operators S_{\pm} , w_1, w_2 the corresponding eigenvectors and suppose that $|\mu| < 1$. If we find $\begin{pmatrix} \alpha_0 \\ \beta_0 \end{pmatrix} \in \text{Preim}_{B_-}(w_1)$ and such that $B_+ \begin{pmatrix} \alpha_0 \\ \beta_0 \end{pmatrix} = k \cdot w_2$ for a constant $k \in \mathbb{C}$ the sequence $\begin{pmatrix} \alpha_{\pm n} \\ \beta_{\pm n} \end{pmatrix}$ converges as $n \rightarrow \infty$.*

Proof. The proof follows directly from the equations (106), (107). By the assumptions $|\mu| < 1$ and the corresponding eigenvector of S_- is w_1 . We chose $\begin{pmatrix} \alpha_0 \\ \beta_0 \end{pmatrix} \in \text{Preim}_{B_-}(w_1)$ and thus $B_- \begin{pmatrix} \alpha_0 \\ \beta_0 \end{pmatrix} = w_1$. The sequence $\begin{pmatrix} \alpha_{-n} \\ \beta_{-n} \end{pmatrix}$ then converges as $n \rightarrow \infty$ thanks to the equation (106).

Similarly $B_+ \begin{pmatrix} \alpha_0 \\ \beta_0 \end{pmatrix} = k \cdot w_2$ and w_2 is an eigenvector of S_+ with the eigenvalue $-\frac{1}{\mu}$, where $|\frac{1}{\mu}| < 1$. The equation (106) then implies convergence of the sequence $\begin{pmatrix} \alpha_n \\ \beta_n \end{pmatrix}$ as $n \rightarrow \infty$. \square

Note 2.1. We will briefly comment on Lemma 2.2.

1. The unitary coin C_0 (49) may produce non-invertible matrices B_{\pm} (100), (101). In fact, we may choose C_0 such that B_{\pm} are not invertible. The determinants of B_{\pm} are:

$$\det(B_-) = -\frac{x_{11}}{s}, \quad (108)$$

$$\det(B_+) = \frac{x_{22}}{s}. \quad (109)$$

If we set

$$C_0 = \begin{pmatrix} 0 & 1 \\ 1 & 0 \end{pmatrix}, \quad (110)$$

both determinants (108) and (109) vanish. Since the coin operator is unitary we either find that both x_{11} and x_{22} are zero or both are non-zero, which implies: the operators B_{\pm} are either both regular or both singular. We will use this observation in the following paragraphs.

2. Going back to the equation (93) describing the eigenvectors of the operators S_{\pm} . We assumed that S_{\pm} are diagonalizable. But in case

$$-\lambda^2 + \sqrt{\lambda^4 + 1} = -\lambda^2 - \sqrt{\lambda^4 + 1} \quad (111)$$

this assumption does not hold. The roots $\lambda_{1,2,3,4}$ of the equation (111) are:

$$\lambda_{1,2} = \pm s(1 + i), \quad (112)$$

$$\lambda_{3,4} = \pm s(1 - i). \quad (113)$$

$$(114)$$

But we have already covered this case while discussing μ_1 as a function of λ (see Figure 3). Plugging any of the roots $\lambda_{1,2,3,4}$ to $\mu_1(\lambda)$ results in $|\mu_1(\lambda_{1,2,3,4})| = 1$. Lemma 2.2 explicitly uses the assumption that $|\mu_1| < 1$.

3. The question of convergence of $\begin{pmatrix} \alpha_n \\ \beta_n \end{pmatrix}$ may be restated as follows: we search $\begin{pmatrix} \alpha_0 \\ \beta_0 \end{pmatrix}$ such that:

$$\begin{aligned} B_- \begin{pmatrix} \alpha_0 \\ \beta_0 \end{pmatrix} &= w_1, \\ B_+ \begin{pmatrix} \alpha_0 \\ \beta_0 \end{pmatrix} &= k \cdot w_2, \end{aligned} \tag{115}$$

for some constant k . Using the equations (100) and (101) we find equations for λ .

We shall investigate under what circumstances there is $\begin{pmatrix} \alpha_0 \\ \beta_0 \end{pmatrix} \in \text{Preim}_{B_-}(w_1)$ satisfying $B_+ \begin{pmatrix} \alpha_0 \\ \beta_0 \end{pmatrix} = w_2$, i.e. under what circumstances are we able to find a solution to the problem governed by the equation (115). We will set:

$$D = \det(C_0) \tag{116}$$

and split our analysis into two cases.

1. If B_{\pm} are invertible, we are to solve the equation:

$$\begin{aligned} &\frac{(-x_{12} - x_{21} - sD + x_{12}\sqrt{\lambda^4 + 1})\lambda^2}{\lambda^2 x_{11} (-\lambda^2 + \sqrt{\lambda^4 + 1})} + \frac{(2s - x_{12})\lambda^4 + Ds(-1 + \sqrt{\lambda^4 + 1})}{\lambda^2 x_{11} (-\lambda^2 + \sqrt{\lambda^4 + 1})} = \\ &\frac{(-2x_{21}s - D)\lambda^2 + D(-1 + \sqrt{\lambda^4 + 1})}{2s\lambda^2 x_{11}}. \end{aligned} \tag{117}$$

2. And when neither B_- nor B_+ are invertible, i.e. x_{11} and x_{22} both zero, we are to solve equations:

$$\begin{aligned} -\frac{sx_{12}}{\lambda^2 - sx_{12}} &= \frac{1}{-\lambda^2 + \sqrt{\lambda^4 + 1}}, \\ \frac{\lambda^2 - x_{21}s}{x_{21}s} &= -\frac{1}{\lambda^2 + \sqrt{\lambda^4 + 1}}. \end{aligned} \tag{118}$$

In order to complete the list we must comment on another dichotomy. The equations above arise when we expect that the eigenvalue μ_1 satisfying $|\mu_1| < 1$ is of the form:

$$\mu_1 = \frac{-\lambda^2 + 1 + \sqrt{\lambda^4 + 1}}{2\lambda s}. \tag{119}$$

The other possibility might have been

$$\mu_2 = \frac{-\lambda^2 + 1 - \sqrt{\lambda^4 + 1}}{2\lambda s} \tag{120}$$

nevertheless the roots of equations (117) and (118) are not affected by the choice of the sign. The set of equations (118) leads to a pair of uncoupled quadratic equations with solutions:

$$\lambda_1 = \pm \frac{1}{s - x_{12}} \sqrt{(s - x_{12}) s x_{12} (2s - x_{12})}, \quad (121)$$

$$\lambda_4 = \pm \frac{-1}{s - x_{21}} \sqrt{(s - x_{21}) x_{21} (2s - x_{21})}, \quad (122)$$

whereas the equation (117) may be rearranged as a quadratic equation in terms of λ^2 . The solutions may be found analytically, for our particular setting with a general coin C_0 the four expected roots are:

$$\lambda_{1,2} = \pm \frac{s \sqrt{(s - Ds - F) \sqrt{F^2 + 4D} + F(D - 1)s + F^2 - 2D}}{\sqrt{Fs + 2D - 1}}, \quad (123)$$

$$\lambda_{3,4} = \pm \frac{s \sqrt{(s - Ds + F) \sqrt{F^2 + 4D} + F(D - 1)s + F^2 - 2D}}{\sqrt{Fs + 2D - 1}}, \quad (124)$$

where $D = \det(C_0)$ and $F = x_{12} + x_{21}$.

Having found roots λ the difference equations (52) and (53) may finally be solved and the convergence of the series (91) can be investigated. We shall refine Proposition (92) based on the gained knowledge regarding roots λ .

Proposition 2.3. *In order to find the eigenvector satisfying (51) we perform the following steps:*

1. *Beginning with a known coin defect C_0 we decide regularity of the boundary operators B_{\pm} using the equations (108) and (109).*
2. *We choose the appropriate equation (117) or (118).*
3. *Having found roots λ we return to the equation (92) describing eigenvectors of the step operator S_{\pm} . Then we examine its eigenvalues (95) and based on their absolute values pick the corresponding eigenvectors $w_{1,2}$ of S_{\pm} .*
4. *If the operators B_{\pm} from the equations (100) and (100) are invertible we proceed as follows. Then set $\begin{pmatrix} \tilde{\alpha}_{-1} \\ \tilde{\beta}_{-1} \end{pmatrix} = w_1$ (we use $\tilde{\alpha}$ etc. because we do not know yet whether the eigenvector could be normalized). Further let $\begin{pmatrix} \tilde{\alpha}_0 \\ \tilde{\beta}_0 \end{pmatrix} = B_-^{-1} \begin{pmatrix} \tilde{\alpha}_{-1} \\ \tilde{\beta}_{-1} \end{pmatrix}$ and $\begin{pmatrix} \tilde{\alpha}_1 \\ \tilde{\beta}_1 \end{pmatrix} = B_+ B_-^{-1} \begin{pmatrix} \tilde{\alpha}_{-1} \\ \tilde{\beta}_{-1} \end{pmatrix}$.*

In case neither B_- nor B_+ are regular, we have:

$$B_- = \begin{pmatrix} 0 & \frac{x_{12}}{\lambda} \\ 0 & \frac{x_{12}}{\lambda} - \frac{\lambda}{s} \end{pmatrix}, B_+ = \begin{pmatrix} \frac{\lambda}{s} - \frac{x_{21}}{\lambda} & 0 \\ \frac{x_{21}}{\lambda} & 0 \end{pmatrix} \quad (125)$$

and thus

$$\begin{pmatrix} 0 & \frac{x_{12}}{\lambda} \\ 0 & \frac{x_{12}}{\lambda} - \frac{\lambda}{s} \end{pmatrix} \begin{pmatrix} \alpha_0 \\ \beta_0 \end{pmatrix} = \beta_0 \begin{pmatrix} \frac{x_{12}}{\lambda} \\ \frac{x_{12}}{\lambda} - \frac{\lambda}{s} \end{pmatrix} = k_1 w_1 = k_1 \begin{pmatrix} \frac{-1}{\lambda^2 - \sqrt{\lambda^4 + 1}} \\ 1 \end{pmatrix}, \quad (126)$$

$$\begin{pmatrix} \frac{\lambda}{s} - \frac{x_{21}}{\lambda} & 0 \\ \frac{x_{21}}{\lambda} & 0 \end{pmatrix} \begin{pmatrix} \alpha_0 \\ \beta_0 \end{pmatrix} = \alpha_0 \begin{pmatrix} \frac{\lambda}{s} - \frac{x_{21}}{\lambda} \\ \frac{x_{21}}{\lambda} \end{pmatrix} = k_2 w_2 = k_2 \begin{pmatrix} \frac{-1}{\lambda^2 + \sqrt{\lambda^4 + 1}} \\ 1 \end{pmatrix}. \quad (127)$$

On the other hand, thanks to the equation (118) for λ we are guaranteed to find a solution. In fact, the non-regularity of B_{\pm} enables us to solve the negative and positive branches of the sequence $\begin{pmatrix} \alpha_n \\ \beta_n \end{pmatrix}$ independently. This is also why we lost the coupling between negative and positive terms and why we found two independent quadratic equations for λ instead of one equation of degree four.

5. Having found $\begin{pmatrix} \tilde{\alpha}_{\pm 1} \\ \tilde{\beta}_{\pm 1} \end{pmatrix}$ and $\begin{pmatrix} \tilde{\alpha}_0 \\ \tilde{\beta}_0 \end{pmatrix}$, we generate the whole sequence $\begin{pmatrix} \tilde{\alpha}_n \\ \tilde{\beta}_n \end{pmatrix}_{n \in \mathbb{Z}}$ by successive application of S_{\pm} . Lemma 2.2 implies this sequence converges as n tends to $\pm\infty$.

6. Finally, we must normalize $\begin{pmatrix} \tilde{\alpha}_n \\ \tilde{\beta}_n \end{pmatrix}_{n \in \mathbb{Z}}$. For both positive and negative branches

$\left\| \begin{pmatrix} \tilde{\alpha}_{\pm n} \\ \tilde{\beta}_{\pm n} \end{pmatrix} \right\|_{n > 1}$ form convergent geometric sequences, we are able to sum easily and thus find the suitable normalizing factor.

Although we could provide explicit formulas for $\begin{pmatrix} \alpha_n \\ \beta_n \end{pmatrix}_{n \in \mathbb{Z}}$ comparable to those derived by Endo and Konno in the equations (74) – (79), we prefer to keep only the outlined guide from Proposition (74). A cumbersome branching and lengthy formulas are thus avoided.

2.4 Phase-altered Hadamard coin and rotations revisited

While comparing eigenvalues gained in the form of roots of the equations (117) and (118) with the equation (59) it is important to note the crucial aspect of the solution proposed by Wójcik et al., namely that their equations yield eigenvalues λ_{\pm} of the square of unitary evolution operator. In order to compare results, one has to take square roots $\sqrt{\lambda_{\pm}}$ and compare them with the roots of our polynomial equations. The results agree perfectly.

With the aim of using the equations (123) and (124) in the following examples, we define:

$$\tilde{D}(X) = \det(X), \quad (128)$$

$$\tilde{F}(x) = x_{12} + x_{21}, \quad (129)$$

where

$$X = \begin{pmatrix} x_{11} & x_{12} \\ x_{21} & x_{22} \end{pmatrix}. \quad (130)$$

We shall calculate squares of $\lambda_{1,2,3,4}$ for an easier comparison. The determinant $\det H$ is -1 and the constant F is $\sqrt{2}$ for the Hadamard coin. Having multiplied H by a factor $k \in \mathbb{C}$ satisfying $|k| = 1$, are led to: $\tilde{D}(C_0) = -k^2$ and $\tilde{F}(C_0) = k\sqrt{2}$. With help of the equations (123) and (124) we find:

$$\gamma_{1,2} = \lambda_{1,3}^2 \pm \frac{(k^2 - k + 1) \sqrt{-k^2} + k(k-1)^2}{2k^2 - 2k + 1}. \quad (131)$$

We may also return to the case studied by Endo and Konno. For their choice of coin defect C_0 (65): $\tilde{D}(C_0) = -1$ and $\tilde{F}(C_0) = 2\sin(\theta)$. Our equations (123) and (124) yield those derived by Endo and Konno in (72).

We will add one more example: suppose we restrict ourselves on a case of a single coin defect of the form:

$$C_0 = R(\theta) = \begin{pmatrix} \cos(\theta) & \sin(\theta) \\ -\sin(\theta) & \cos(\theta) \end{pmatrix} \quad (132)$$

Here we fix $D = 1$ and $F = 0$. This case is thus particularly simple to investigate. Equations (123) and (124) imply:

$$\lambda_{1,2} = \pm i. \quad (133)$$

We have just seen an interesting case: a subgroup of $U(2)$ leaving the roots λ unchanged was found. Furthermore, we only have two distinct roots. Going back to the equations (117), (118), we may revert our steps and use $\lambda = \pm i$ as a starting point. Examining each case we arrive at a necessary condition for obtaining $\lambda = \pm i$:

$$x_{11}x_{22} = (x_{21} - 1)(x_{12} - 1) \quad (134)$$

or expressed with determinant:

$$\det(C_0) = 1 - x_{12} - x_{21}. \quad (135)$$

This condition is certainly satisfied for rotation defects.

2.5 Possible generalizations

To conclude this section a note on possible generalizations will be added. We have seen an analytical solution to the eigenvalue problem concerning a single coin defect on the Hadamard walk. The operators S_{\pm} proved to provide a deep enough insight, so that we may find stationary states of the perturbed Hadamard walk using their spectra. Can we repeat the procedure for multiple coin defects? We do not know. But we will summarize knowledge we gained regarding this issue. We will address results obtained using numerical simulations to make assumptions regarding the analytical solutions and their properties. Any details concerning implementations will not be included here, we will discuss this topic separately in the Section 3.1. Right now we state only that numerical simulations agree very closely with analytical solutions for single coin defects and we suppose simulations provide reliable results even in cases we are not able to confirm analytically. Though, we point out that the numerical analysis is limited to only finite systems with the periodic boundary condition. We are thus not able to analyze eigenvalues from the continuous spectrum of the Hadamard walk. Nevertheless, the coin defects introduced usually isolate certain eigenvalues from the continuous spectrum. Only for such eigenvalues are we able to state that finite and infinite model agree.

Remark 2.1. Summary of our knowledge regarding multiple coin defects.

1. Lemma 2.2 may be restated for two directly neighbouring coin defects. The resulting polynomial equations to be solved are unfortunately of high degree – we usually arrive at equations of degree 6 in λ^2 – and we are not aware of any method that would provide us solution. What is even worse: this case tends to be hard even if we add assumptions such as: the coin defects are of the same kind or even exactly the same. Previously easy-to-solve cases remain unsolved when we examine directly neighbouring defects.
2. While introducing defects if the same kind we in general not able to use any knowledge in regard to the single coin case. For example single coin defect in the form (133) introduces roots $\lambda_{1,2} = \pm i$. But a perturbed Hadamard walk with two neighbouring $\frac{\pi}{4}$ -rotations has four stationary states with eigenvalues $\lambda_{1,2} \approx \pm(0.3162+0.9487i)$ and $\lambda_{3,4} \approx \pm(0.3162-0.9487i)$. This brings a new phenomenon: while varying the angle of rotation, spectral properties of the Hadamard walk with two coin defects change too. When we introduce two neighbouring $\frac{\pi}{3}$ -rotations, the eigenvalues caused by the perturbation will be $\tilde{\lambda}_{1,2} \approx \pm(0.2257 + 0.9742i)$ and $\tilde{\lambda}_{3,4} \approx \pm(0.2257 - 0.9742i)$. We thus infer that two neighbouring rotations might introduce up to four stationary states and their eigenvalues tend to follow a clear symmetry. This suggests we are actually unable to uncover the right equations to solve.
3. If we choose to introduce two distinct directly neighbouring coin defects we may obtain two or four roots although we are to solve equations of higher degree. Hadamard coin with a rotation gives rise to only two distinct roots. This case should actually not be considered as two coin perturbations. On the other hand, any formalism describing multiple coin defects should direct us to the cases already studied. We thus allow for using the Hadamard coin in multiple coin perturbations. If we fix the angle $\theta = \frac{\pi}{3}$ in the coin (65) proposed by Endo and Konno and add a rotation with the same θ , we still obtain only two roots.

An example with four roots may be constructed using iH and $iR(\theta)$ in the direct vicinity.

Throughout our experiments we did not encounter any combination of coin defects in the direct neighbourhood that would give rise to more than four eigenvalues. We suppose that developing a theory of mappings between eigenvectors of the operators S_{\pm} based on multiple coin defects would provide an important insight. Despite multiple attempts to investigate compositions of mappings arising from a direct generalization of the proposed solution, we were not successful in lowering the degree of the resulting equations.

4. The previous case could be regarded as two coin defects with a separation of the length 1. Another important case to study takes into account separation of the length 2. In the following paragraphs we always assume that the distance between two coin defects is two nodes.

A combination of $R(\theta_1)$ and $R(\theta_2)$ gives rise to four roots. Cases concerning iH and $iR(\theta)$ have six roots for various choices of θ . We did not encounter any two coin perturbation that would isolate 8 eigenvalues from the continuous spectrum.

The final remark regarding two coin perturbations with separation two discusses symmetries. From our observations of numerical simulations, the problem of finding roots of this particular setting shall lead to a cubic polynomial in λ^2 . In all cases studied numerical methods have implied: if λ is an eigenvalue corresponding to a two-coin defect, so is $-\lambda$.

5. When we increase the separation further new phenomena occur again. For the case of two coin defects $iR(\theta)$ where $\theta = \frac{\pi}{4}$ we have:

separation	1	2	3 and more
number of roots	4	4	8

Table 1: Number of roots for two-coin defect: $iR(\theta)$ where $\theta = \frac{\pi}{4}$.

Nevertheless, setting two coin defect $iR(\theta_{1,2})$ where $\theta_1 = \frac{\pi}{4}$ and $\theta_2 = \frac{\pi}{3}$ leads to:

separation	1	2	3 and more
number of roots	4	6	8

Table 2: Number of roots for two-coin defect: $iR(\theta_{1,2})$ where $\theta_1 = \frac{\pi}{4}$ and $\theta_2 = \frac{\pi}{3}$.

In spite of having this simple relation for separations greater than than two nodes, the roots do not remain constant. As the distance between coin defects increases, the roots tend to those determined by the single coin defect equations (123) and (124). We provide numerically determined eigenvalues corresponding to the latter case for the separation of three nodes ⁷:

roots	$\lambda_{1,2}$	$\lambda_{3,4}$
approx. values	$\pm(0.6416 + 0.7670i)$	$\pm(0.6242 - 0.7813i)$
roots	$\lambda_{5,6}$	$\lambda_{7,8}$
approx. values	$\pm(0.5612 - 0.8277i)$	$\pm(0.5486 + 0.8360i)$

Table 3: Roots for two coin defects $iR(\theta_{1,2})$ where $\theta_1 = \frac{\pi}{4}$ and $\theta_2 = \frac{\pi}{3}$ with separation 3.

The impact of separation between two coin defects on the spectrum investigated is even clearer when plotted. See Figure 4 or the case of two $\frac{\pi}{4}$ rotational coins.

⁷The eigenvalues were rounded to four decimal places.

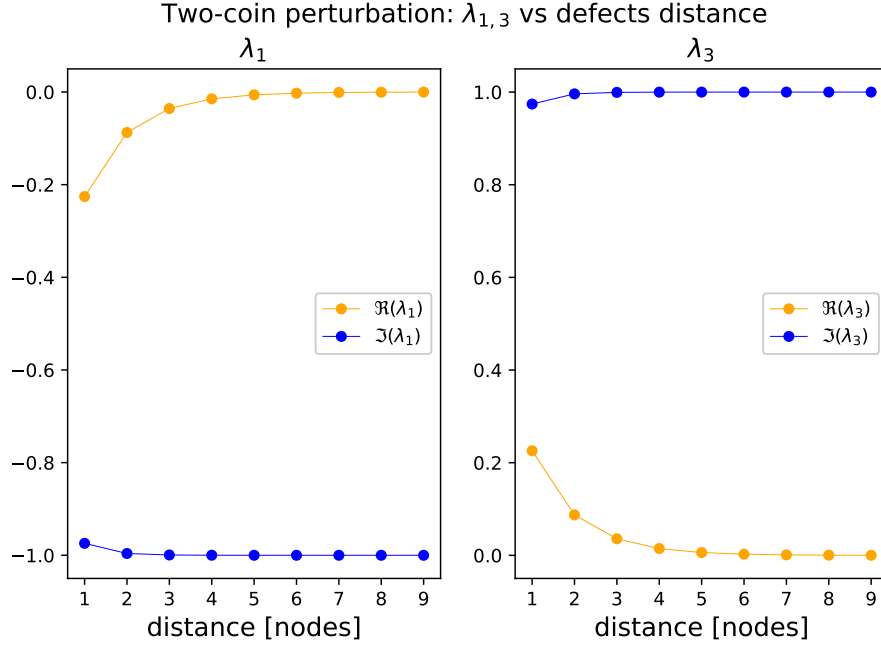


Figure 4: By examining two-coin perturbations numerically we found interesting relations between resulting spectra and distances between defects discussed. As an example we plotted the eigenvalues λ_1 and λ_3 for two $\frac{\pi}{4}$ -rotations. Surprisingly, even small separation of circa eight nodes “unties” the defects and they start to act as if they were independent. Note that by adding the dimensions of the corresponding eigenspaces an invariant is obtained. However, examining numerical simulations, we find that multiplicities are not being conserved: for small separations we find four distinct one-dimensional eigenspaces. The further the defects are, the closer is the separation between eigenvalues, and we are usually not able to discern between the paired eigenvalues for distances $\gtrsim 20$ due to numerical precision. We thus obtain two two-dimensional eigenspaces.

3 Numerical solutions for the Hadamard walk

3.1 Outline of the simulation

In order to study discrete quantum walks numerically we chose to model quantum walks on finite lattices. Discussion of additional boundary conditions due to creating finite models of originally infinite problems is described in the Section 2.1. Periodic boundary conditions were studied primarily, even though other types were implemented as well. Our aim was to benefit from computational power computers offer, to simulate adiabatic changes of the evolution operator keeping track of its eigenvalues, their corresponding eigenstates and to visualise resulting probability distributions. We thus decided to design a framework that would mirror the physical objects as digital structures. We will leave details concerning programming structures to the Section A.1 and aim to describe mathematical concepts used to perform simulations in the following paragraphs.

We did not intend to restrict defects on the finite Hadamard walk to only coin-space defects. Thus our implementation of adiabatic transitions may connect any two evolution matrices U_1 and U_2 via a path in $U(2N)$, where we denote the number of nodes N and use conventions described in the Section 2.1⁸. Although the algorithm for finding trajectories in $U(2N)$ allows for transition between general unitary matrices, we imposed an additional criterion: while performing transitions between two operators with defects only in the coin space, the trajectory has to respect the structure of the Hadamard walk and we must not introduce any other kind of defects. On the other hand we admit co-existence of multiple coin perturbations at different locations. For example while moving a perturbed coin from a location n to a new location $m \neq n$, we may observe two defects at once while following the path of adiabatic transition.

Due to the finiteness of the simulated Hadamard walk we absorb the boundary conditions from the Section 2.1 in the evolution matrices. Although we are able to perform a change of boundary conditions during the evolution, we did not direct much attention at this kind of transition.

Imagine that we are given a unitary evolution operator U_1 describing a Hadamard walk with the periodic boundary. We would like to slowly perturb the coin located at position n . To be more precise, we begin with a coin $C_n = H$ and ask the computer to calculate a transition $H \mapsto D_n$. We shall write coin space operators corresponding to U_1 as C_i , where $i \in \widehat{N-1}$; operators D_i , on the other hand, correspond to the unitary evolution U_2 . Written formally:

$$\begin{aligned} C_i &= D_i \quad \text{for } i \neq n, \\ C_n &= H \\ D_n &\in U(2). \end{aligned} \tag{136}$$

Being in time t_0 of the simulated evolution governed by U_1 , we search for a path from U_1 to U_2 . We may also dictate the number of steps $T \in \mathbb{N}$ the transition will take. It is convenient to introduce a time-dependent evolution operator $U(t)$ with coin space operators P_i , $i \in \widehat{N-1}$. In this particular setting, our requirement not to break the

⁸In order to simulate evolution of a walker on N nodes, we are required to keep track of $2N$ coordinates.

structure of the Hadamard walk becomes formally:

$$\begin{aligned} \forall s \in \widehat{T} : P_i(t_0 + s) &= C_i \quad \text{for } i \neq n, \\ \forall s \in \widehat{T} : P_n(t_0 + s) &\text{ interpolates between } C_n \text{ and } D_n. \end{aligned} \quad (137)$$

One way to satisfy conditions outlined in (136) is to calculate the interpolation between C_n and D_n in $U(2)$. The time-dependent evolution operator could then be calculated easily as a finite version of (48). A generalisation of this approach would enable us to consider cases such as moving the coin defect from the position n to m . The only difference we would have to take into account was the number of interpolations: two simultaneous interpolations were required.

The interpolation $P_n(t_0 + s)$ between C_n and D_n may be written as follows:

$$\begin{aligned} P_n(t_0) &= T(t_0)C_n \stackrel{!}{=} C_n, \\ P_n(t_0 + T) &= T(t_0 + T)C_n \stackrel{!}{=} D_n, \\ P_n(t_0 + s) &= T(t_0 + s)C_n. \end{aligned} \quad (138)$$

Although the equation (138) may seem to introduce as unnecessary formalism it transforms the problem of connecting two arbitrary points in $U(2)$ to a simpler one: the task is to find a path between $T(t_0) = I$ and

$$T(t_0 + T) = D_n C_n^{-1}, \quad (139)$$

because C_n and D_n are unitary. We will construct the path $T(t_0 + s)$ in Proposition 3.1.

Proposition 3.1. *In order to connect two arbitrary unitary matrices in $U(2)$ we may follow the guide:*

1. *Diagonalize $D_n C_n^{-1} = V E V^\dagger$ and denote eigenvalues of the operator E $\exp(i\eta_1)$, $\exp(i\eta_2)$. We follow the convention to choose the argument of a complex number in the range $(-\pi, \pi]$.*
2. *Set $\tilde{E} : [0, 1] \rightarrow U(2)$ to be:*

$$\tilde{E}(p) = \begin{pmatrix} \exp(ip\eta_1) & 0 \\ 0 & \exp(ip\eta_2) \end{pmatrix}. \quad (140)$$

3. *We define $T : [t_0, t_0 + T]$ as follows:*

$$T(t_0 + s) = V \tilde{E}(f(s)) V^\dagger, \quad (141)$$

where the increasing function f maps the interval $[t_0, t_0 + T]$ onto $[0, 1]$. Note that we may adjust the speed of passage both by the choice of its length T and via the parametrization f . The typical choice for f is:

$$f(s) = \begin{cases} 0 & \text{for } s \leq t_0. \\ \frac{s-t_0}{T} & \text{for } s \in (t_0, t_0 + T), \\ 1 & \text{for } s \geq t_0 + T. \end{cases} \quad (142)$$

A similar technique may be used to find paths directly between the operators U_1 and U_2 governing the evolution of the Hadamard walk before and after a perturbation. Thanks to the structure of the operators U_1 and U_2 described in the equation (136) the product $U_2U_1^\dagger$ is very close to a unit matrix; the only dissimilarities from I are in the vicinity of the elements of the modified coins. To be more precise, while introducing a new coin defect at location n , we encounter perturbations of matrix elements at positions $[2n, 2n]$, $[2n, 2n + 5]$, $[2n + 5, 2n]$, $[2n + 5, 2n + 5]$, where the square bracket denotes rows and columns. The calculation of $U_2U_1^\dagger$ is thus rather fast and straightforward. Adiabatic passages are then calculated using the eigenvectors V of $U_2U_1^\dagger$. Although we perform the diagonalization only once – while introducing or modifying a defect – this step may require significant amount of computer resources. But why should we take the trouble to perform a more difficult task when Proposition 3.1 solves our problem?

1. We aimed to create a simulator offering general transitions, such as introduction of different boundary conditions or topological changes of the lattice. The latter mentioned encompass for example a creation of new cycles swapping nodes etc. It is also important to note that for defects in coin space the more general approach concerning evolution operators $U_{1,2}$ gives exactly the same interpolation (or possibly multiple interpolations) as outlined in Proposition 3.1. We are thus able to provide a general method governing transitions between evolution operators that respects our requirements (137). On the other hand we increase our demands on computers because we need to multiply larger matrices during transitions ⁹.
2. Bearing in mind that we shall examine spectra of operators undergoing adiabatic transitions, we benefit from direct access to their matrices as whole. With the intention of finding all their eigenvalues and tracking eigenspaces, having an element-wise access to their matrix representation simplifies the task significantly.

It is also important to note that eigenvalues to be computed have all the same absolute value due to the unitarity and their separation is very subtle. Consider for example Hadamard walk on 1000 nodes. We thus need $2 \cdot 1000$ coordinates and expect to find 2000 eigenvalues. Assuming the best case scenario, the eigenvalues follow an equidistant distribution ¹⁰ and this leads us to $\frac{\pi}{1000}$ radians difference in arguments of neighbouring eigenvalues. The numerical method chosen thus must be designed carefully and with respect to very close separation of eigenvalues. Furthermore, the set of eigenvectors must be orthonormal.

3.2 Adiabatic transitions

In the section 2.2 we have seen an analytical solution of the eigenvalue problem (51). One of our aims was to investigate adiabatic perturbations introducing coin defects. In Wójcik model[2] we have seen not only analysis for defects concerning the phase-altered Hadamard coin but also an interesting result concerning the walker. If we initialize the walker in the state (32) centered around the coin defect, part of its state stays

⁹The overhead is actually not so significant while working with modern CPU architectures providing vector instructions such as AVX2. Although we still need to perform matrix multiplication of potentially large ($\approx 10^4$ rows) matrices we are able to perform the multiplication relatively efficiently. Assembling the matrices, on the other hand, in place disallows us using vectorized instructions in our case.

¹⁰This assumption does not hold and the resulting separation is thus even worse.

trapped around the origin. We would like to examine more general cases and discuss slow transitions between defects, adiabatic shift of a coin defect to a neighbouring node, adding a new defect etc.

In Figure 5 we present a snapshot of state functions for two walkers. Remind that we may use coordinates $\begin{pmatrix} \alpha_n \\ \beta_n \end{pmatrix}_{n \in \widehat{N-1}}$; thus a two-color scheme is used so that we may distinguish between α 's and β 's. We will always follow the rules:

- Note 3.1.**
1. The walker on the left is called the reference walker and it visualizes scenarios as if we did not introduce any defect.
 2. The walker on the right is called the perturbed walker and it visualizes scenarios taking into account all defects introduced.
 3. Both walkers were introduced with the same initial conditions and they do not share the lattice. However, their lattices are of the same size and satisfy the same boundary condition.
 4. Unless stated otherwise, we chose the symmetric initial state (32) shifted to the centre of the grid.
 5. Although that the more traditional way is to plot the probabilities of finding the walker at the n -th node $\left\| \begin{pmatrix} \alpha_n \\ \beta_n \end{pmatrix} \right\|^2$, we opted for plotting $\|\alpha_n\|^2$ and $\|\beta_n\|^2$ separately. α 's are plotted orange and β 's are in blue color.
 6. Coin defects are marked using vertical lines. An active coin defect is shown by a red dashed line whereas we mark by a green dotted lines places where a defect had been introduced but is not present anymore.

Figure 5 shows a “trapped” walker on a 100-node periodic grid. The coin defect had been introduced just before the walk started. $iR(\theta)$ coin perturbation with $\theta = \frac{\pi}{6}$ ¹¹ was chosen. Note that the perturbation is one node off-centre.

¹¹Although the value $\frac{\pi}{6}$ is not distinctive anyhow, we performed a significant amount of numerical simulations in this setting. Everybody uses $\frac{\pi}{4}, \frac{\pi}{2}, \dots$ but no one picks $\frac{\pi}{6}$. The number 6 is thus sad and we wanted to cheer it up a little bit.

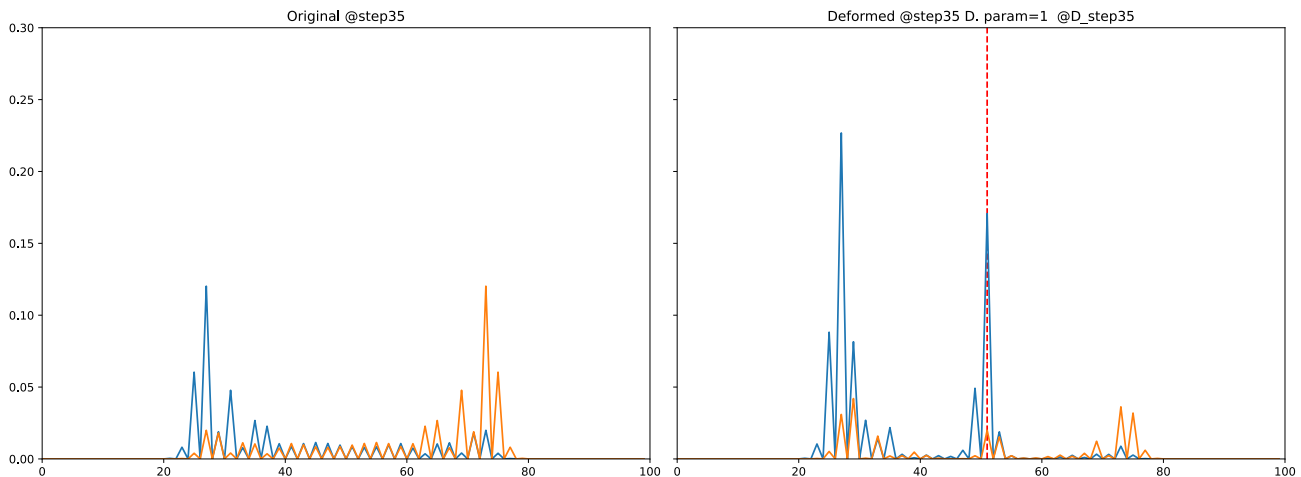


Figure 5: A comparison of two 100-nodes Hadamard walks. We may regard the reference walker in the left plot after having performed 35 steps from the initial state (32). Although the perturbed walker was initialized in the same initial state, part of its probability is trapped due to the coin defect $iR(\theta)$, where $\theta = \frac{\pi^i}{6}$.

Throughout our path to the analytical solution (123) (124) of the eigenvalue problem (51) concerning the Hadamard walk with a single coin perturbation we used to check intermediate results using numerical simulations. Having derived the analytical solutions we could finally test the precision of simulations and especially our ability to give numerical estimates to the eigenvalue problem. For single coin perturbations the results agree perfectly. We are furthermore able to provide numerical analysis of stationary states and create predictions regarding resulting spectra as mentioned in the Remark 2.1.

The impact of the periodic boundary condition will be discussed with the help of Figure 6. It shows a sample eigenvector corresponding to a $\frac{\pi}{4}$ -rotation coin defect. Remind Proposition 2.3 implied that we shall see a geometric sequence while examining the norms $\left\| \begin{pmatrix} \alpha_n \\ \beta_n \end{pmatrix} \right\|^2$. The numerically determined eigenvectors satisfy this property. Furthermore, they tend to zero fast enough that their interaction with the periodic boundary is negligible. We may also spot the irregularities in plot of the phase. We anticipate to see a periodic phase dependency. The numerical solution confirms our expectations to a certain extent: in the neighbourhood centered around the position of the perturbation considered, the phase follows the periodic pattern. But as soon as we move ≈ 40 steps away the regularity of phase disappears. This effect is due to the round-off error caused by multiplication of extremely small numbers. Such fast convergence to zero is to our benefit: we do not need to include the interaction with the boundary if we stay far enough from it.

We may also start the non-perturbed Hadamard walk and introduce the coin perturbation slowly. A 20-step adiabatic transition that introduces a the same $\frac{\pi}{4}$ -rotation coin shall be presented. In the following paragraphs operator $U(t)$ governing the evolution of the Hadamard walk will be time dependent. We performed 40 steps of an unperturbed walk, i.e. $U(t)$ was constant, and beginning with the 40th step we slowly interpolated from the Hadamard coin to a $\frac{\pi}{4}$ -rotation using the linear parametrization (142). In Figure 7 four snapshots of the evolution of its spectrum are shown. With the aim to use a finite-dimensional system as an approximation to an infinite one and bearing in mind

A sample eigenvector for $\pi/4$ rotation coin defect

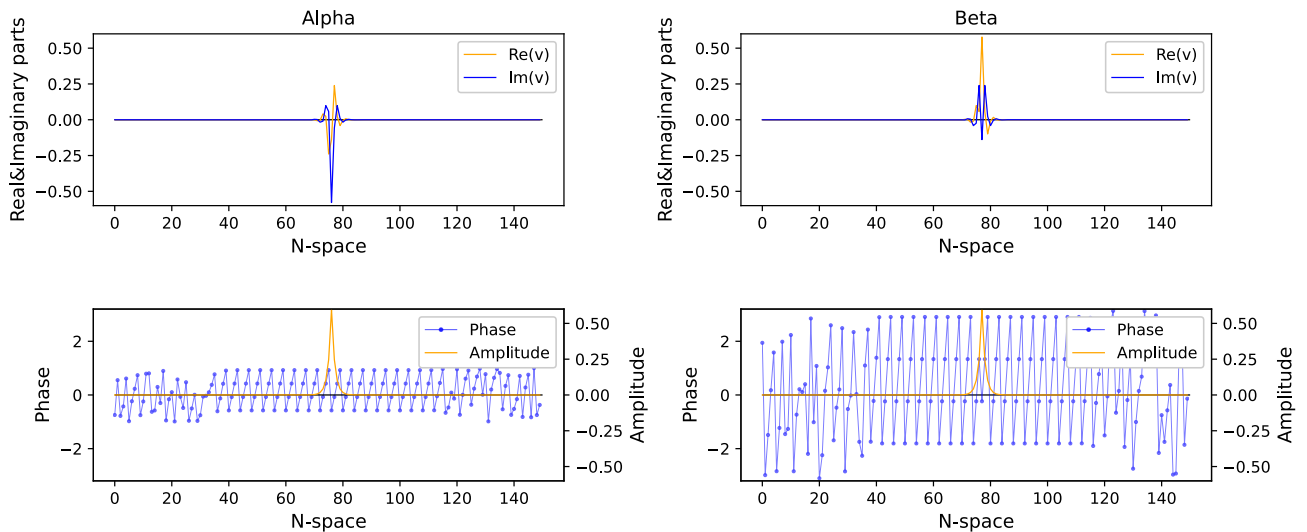


Figure 6: A sample eigenvector corresponding to a $\frac{\pi}{4}$ -rotation coin defect. As Proposition 2.3 anticipate the amplitudes follow a geometric sequence.

that according to the Lemma 2.2 the operators S_{\pm} must have an eigenvalue satisfying $|\mu| < 1$. But we have shown this requirement implies:

$$\arg(\lambda_{1,2}) \in \left(\frac{\pi}{4}, \frac{3\pi}{4} \right) \cup \left(-\frac{3\pi}{4}, -\frac{\pi}{4} \right). \quad (143)$$

These eigenvalues were thus highlighted.

While comparing the analytical and numerical solutions of stationary states for various perturbations we also compared the analytical and numerical calculation of the eigenvalues (123) (124) during transitions. A sample plot showing the four roots that arise while introducing $iR(\theta)$ coin perturbation, where $\theta = \frac{\pi}{6}$, is shown in Figure 8. Several these plots were made in pairs: we always calculated the same transition both analytically and numerically. The results agree beyond our expectations. It is in fact impossible to distinguish between eigenvalues thus obtained.

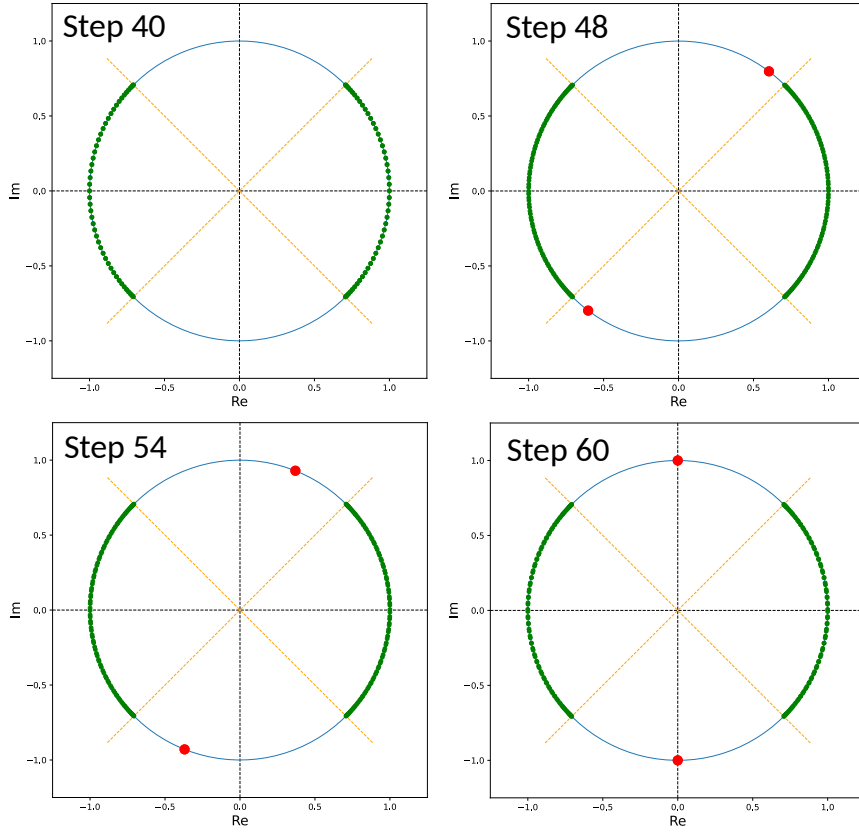


Figure 7: Having performed 40 steps of unperturbed Hadamard walk, we introduced a rotational coin defect and tracked eigenvalues during a 20-step transition. Eigenvalues marked by green dots lying on the left and right semi-arcs are present even without presence of any defect. This is due to the periodic boundary condition. On the other hand eigenvalues $\lambda_{1,2}$ marked red are introduced thanks to the perturbation and their arguments satisfy the condition $\arg(\lambda_{1,2}) \in (\frac{\pi}{4}, \frac{3\pi}{4}) \cup (-\frac{3\pi}{4}, -\frac{\pi}{4})$. Compare the plot with Figure 3 where we divided the unit circle based on relations between eigenvalues $\mu_{1,2}$ (95) of the operators S_{\pm} and candidates for eigenvalues λ .

Paths of selected eigenvalues of the Hadamard walk: analytical solution

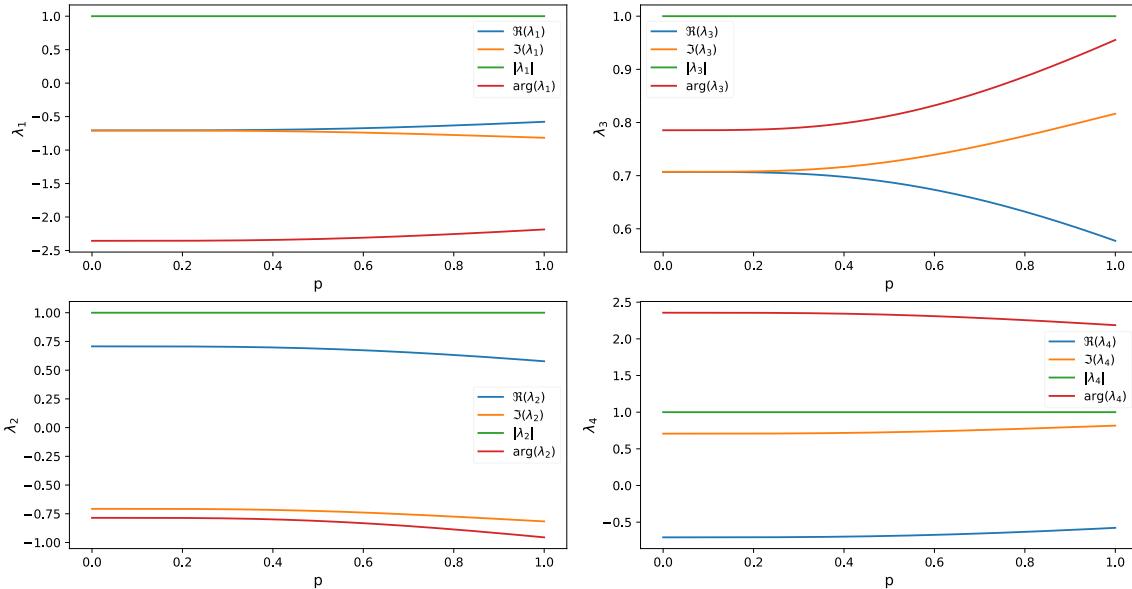


Figure 8: Analytically calculated paths of the eigenvalues that arose due to an adiabatically introduced coin perturbation. In this case an imaginary rotation $iR(\theta)$ with $\theta = \frac{\pi}{6}$ was introduced. Instead of fixing a time interval and picking up a parametrization, e.g. (142) we chose to plot the transition using the dimensionless time p .

3.3 Perturbation shift

We made several attempts at generalizing our analytical solution to the eigenvalue problem to the case of multiple defects. A short summary of known properties of multiple coin defects is in the Remark 2.1. Several cases concerning particular settings or combinations of perturbations have been studied using numerical simulations. Multiple coin defects and particularly multiple coin defects in close vicinity are an important feature of adiabatic transition concerning shifting of the perturbations.

Imagine a coin defect C_n was introduced at a position n . Our task is to move the defect one node left or right. For example if we consider the partially trapped walker from Figure 5, we may ask whether we could shift the probability peak to a neighbouring node moving the trapped state align. We might certainly reset the coin C_n to the Hadamard coin H and then introduce a new perturbation at the location $n - 1$ or $n + 1$. This procedure is not, however, efficient: while we take away the coin perturbation at the node n , we also lose the walker's localization. We may try to improve this method by designing a direct transition between two Hadamards with a single-coin defect. Though, this approach enforces a co-existence of a pair of coin defects in close vicinity.

We shall begin by presenting two examples. Both of them implement the idea of the direct transition between two Hadamard walks with single-coin perturbation initialized in the symmetric state (32). In the first example we provide a demonstration that the method outlined in the paragraphs above is vivid and we may actually move the walker to a neighbouring node. Then we will present an example where we fail to shift the probability peak as desired. We actually manage to do the contrary – the peak vanishes completely. In both experiments the walkers underwent the same adiabatic transition: after having performed 20 steps of a perturbed walk with a single coin defect located at the node 76 we initialized a 10-steps adiabatic passage in order to slowly push the coin perturbations to the node 77.

In the first setting we fixed:

$$C_{76}^A = D_{77}^A = i \begin{pmatrix} \cos(\theta) & \sin(\theta) \\ -\sin(\theta) & \cos(\theta) \end{pmatrix}, \quad (144)$$

where $\theta = \frac{\pi}{4}$. The second experimental setup considered the same coin defects except for a phase change:

$$C_{76}^B = D_{77}^B = \begin{pmatrix} \cos(\theta) & \sin(\theta) \\ -\sin(\theta) & \cos(\theta) \end{pmatrix}. \quad (145)$$

The choice for θ remained unchanged. We shall refer to the walkers from the setting one as A -walkers and to those from the setting two as B -walkers. Even though the initial states of the perturbed A - and B -walkers depicted in Figure 10 and Figure 13 seem comparable – the probability peak is present in both cases and both walkers experience slight asymmetry due to the initial position of the perturbed coin defect – during the passage their evolution bifurcates dramatically.

Note that the imaginary rotation introduces 4 eigenvalues whereas the regular rotation only 2. Throughout the transition of A -walker we have 4 eigenvalues and their paths are relatively smooth – see Figure 12. On the other hand, while regarding the trajectories of B -walker's eigenvalues we begin with only two eigenvalues, two more eigenvalues are suddenly appear in the 3rd step and finally in the 8th step we suddenly lose the eigenvalues corresponding to the coin space perturbation. The paths of the B -walker are depicted in Figure 15.

After having passed the transitions, both walkers A and B perform ten more steps as shown in Figure 11 and Figure 14. We managed to shift the probability peak A -walker started with. In contrast, B -walker's localization was not preserved. The transition actually destroyed the probability peak and dispersed it into the neighbourhood of the shifted defect.

It is up to the designer of the adiabatic transition whether such behavior is or is not desired. We would like to point out that only 10-step transition suffice to almost eliminate the chance to find the walker in the new location. After the passage the probability of finding the walker at the new location is $\approx 0.09\%$. Note that we begun with the probability $\approx 8\%$. An alternative visualisation of paths to that offered in Figure 15 is presented in Figure 9. Visualising the paths directly on the unit circle provides us usually with a slightly different insight. While observing trajectories depicted in Figure 9, it is easy to spot an interesting pattern: beginning with the eigenvalues $\pm i$ typical for rotations, we see the original pair tends to rotate counterclockwise and a pair of new eigenvalues appears at the boundary of the continuous spectrum. As the passage progresses, the original eigenvalues merge with the continuous spectrum whereas the newly appeared pair tends to $\pm i$. Finally, the original spectral properties are restored. But we managed to carry the original probability peak away to the subspace corresponding to the finite approximation of the continuous parts of the spectrum.

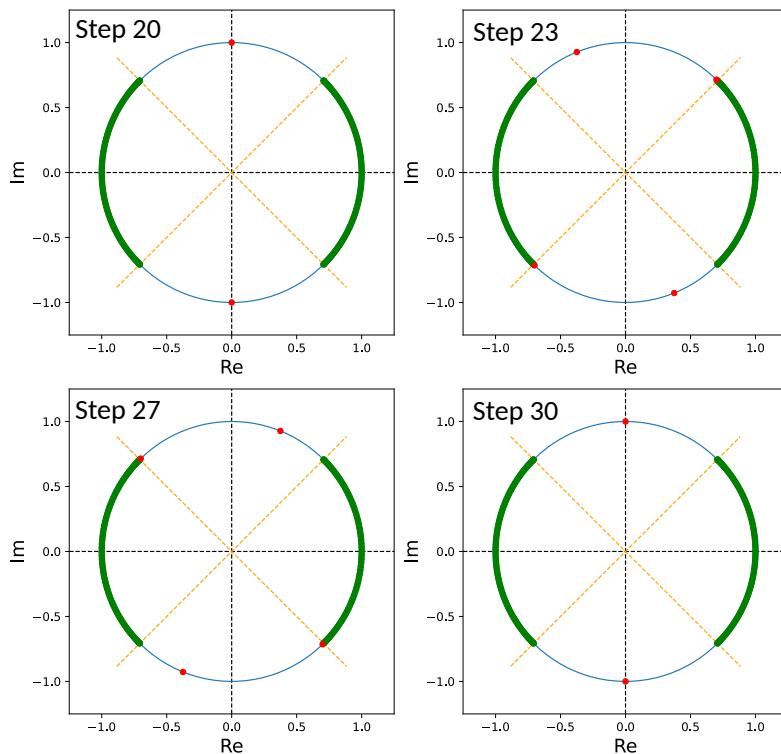


Figure 9: While performing an adiabatic transition between two rotation coin defects, two new eigenvalues suddenly appear in the beginning and later – by the end of the adiabatic passage vanish.

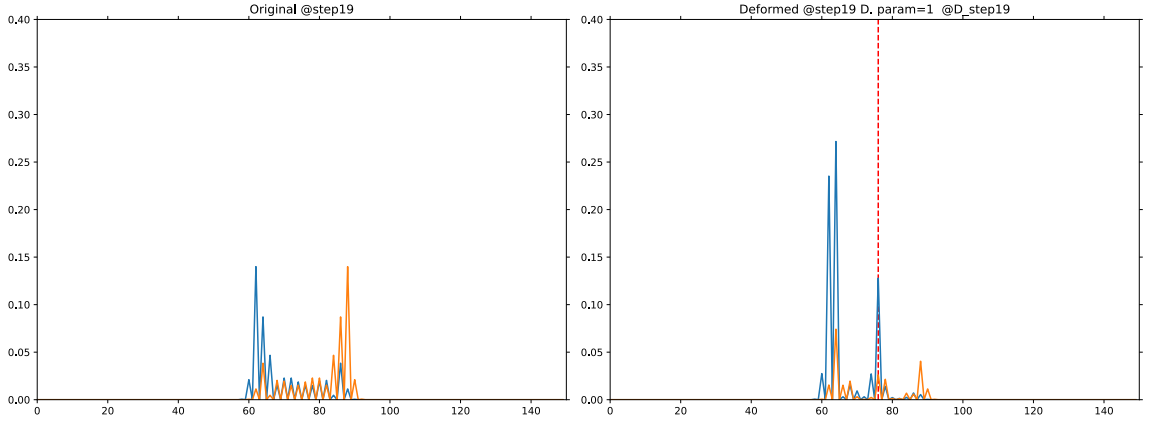


Figure 10: A-walker after 20 steps of perturbed evolution with the coin C_{76}^A (144). The probability is clearly peaked around the location of the perturbed coin.

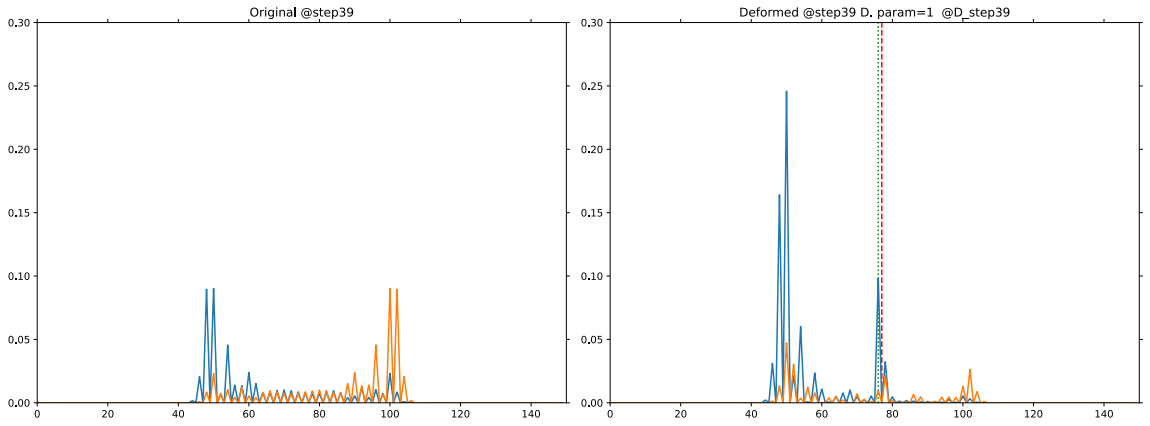


Figure 11: A-walker after 10 steps transition steps followed by 10 steps of evolution with the coin D_{77}^A (144). The probability remained peaked around the location of the shifting perturbation.

Perturbation shift by 1 node: imaginary rotation

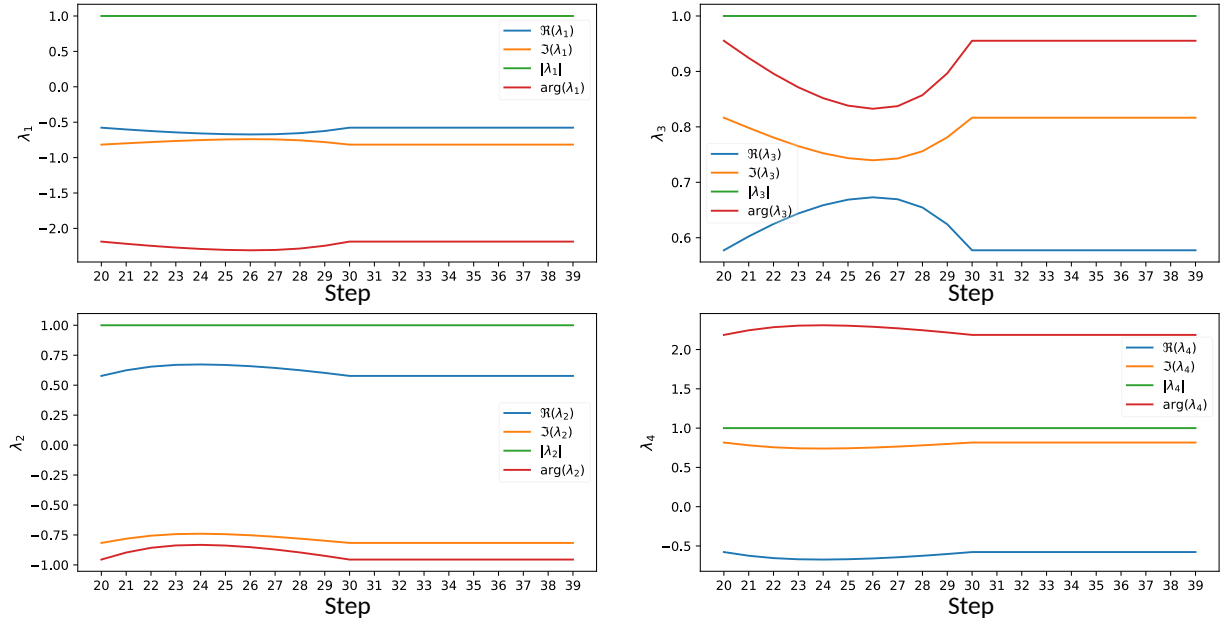


Figure 12: Numerical calculation of the paths taken by the selected eigenvalues under the coin shift. In the case of $iR(\frac{\pi}{4})$ we do not observe any dramatic dynamics.

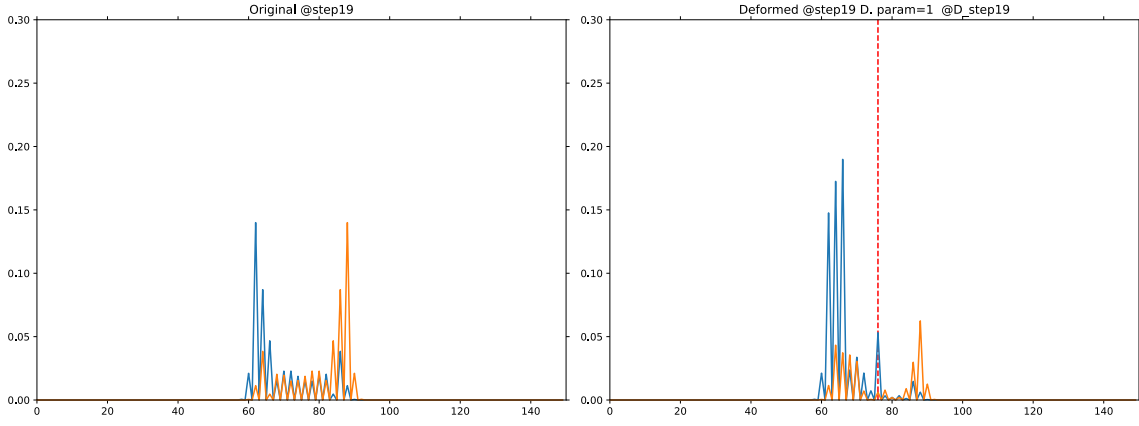


Figure 13: B -walker after 20 steps of perturbed evolution with the coin C_{76}^B (145). B -walker's probability is also peaked around the location of the coin defect.

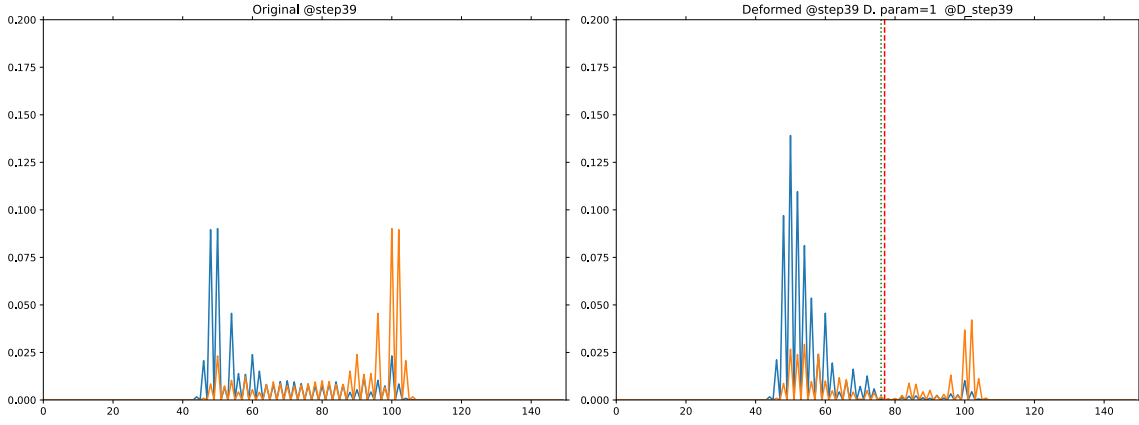


Figure 14: B -walker after the 10-step transition steps followed by 10 steps of evolution with the coin D_{77}^B (145). We managed to destroy the probability peak in the vicinity of the shifted perturbation. When we examine the probability to find the perturbed B -walker at the node 77 in time, we find that the probability is almost zero.

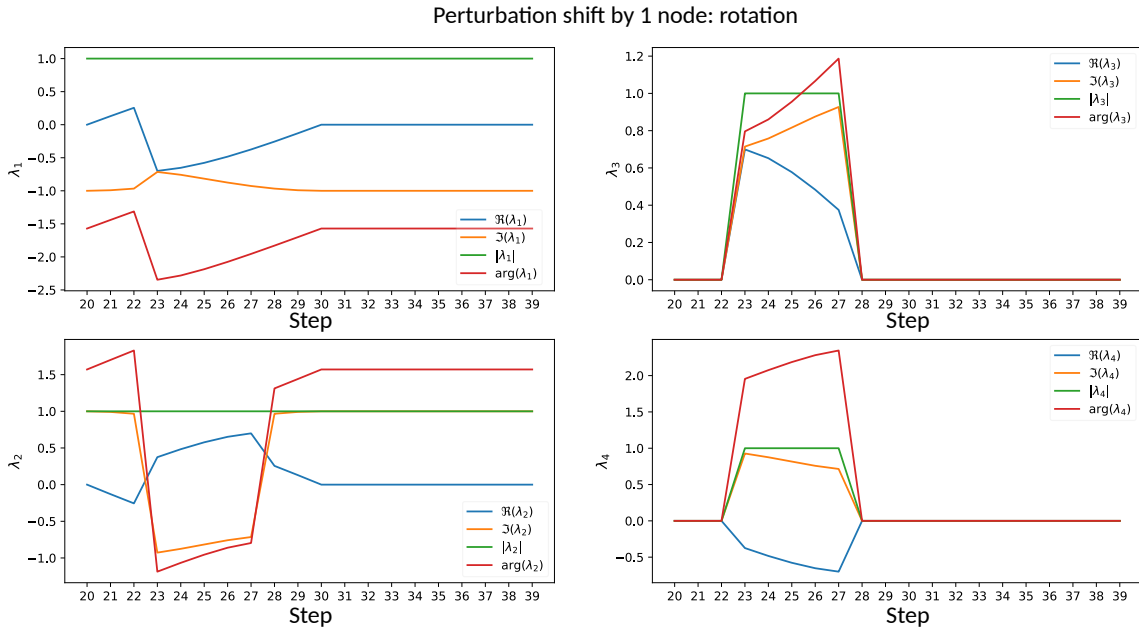


Figure 15: Numerical calculation of the paths taken by the selected eigenvalues under the coin shift. The case of $R(\frac{\pi}{4})$ introduces a turbulent dynamics and we observe an emanation of two previously non-existent eigenvalues during the transition. Furthermore, the probability peak is carried away to the eigensubspace corresponding to the finite approximation of continuous spectrum which is the exact opposite we wanted to achieve. Or is it?

Imagine we track an a trapped walker. The walker is *trapped* because part of it state has a non-zero projection onto an eigensubspace or possibly eigensubspace of the unitary evolution. If we slightly perturb the spectrum of the time step operator, we expect that the eigensubspaces would not change drastically. Although the the classical statements of the AT introduced in Section 1.3 propose statements about the adiabaticity based on properties of Hamiltonians, we may try to perform comparably small perturbations considering the discrete evolution of the Hadamard walk. Even though we might try to perform transitions very slowly, we may never escape the inherent discreteness imposed by the step operator. Our experiments, on the other hand, suggest we could benefit from adjusting rates of the passages.

In order to express the rate of adiabaticity we introduced several metrics.

1. One possibility is to track projections onto the eigensubspaces corresponding to the eigenvalues isolated from the continuous spectrum (or its approximation in the finite case). We are then interested in examination of their consecutive application. Numerical simulations enable us to do so. We introduce the following function:

$$\Xi_{\lambda_1, \dots, \lambda_n}(t_0, t_1) = \left\| \prod_{i=t_0}^{t_1} P_{\lambda_1, \dots, \lambda_n}(i) \right\|, \quad (146)$$

where we consider instantaneous eigenvalues $\lambda_{1, \dots, n}$ to be functions of the discrete time and we denote the projector onto the eigensubspaces corresponding to the eigenvalues $\lambda_{1, \dots, n}$ at the time step j $P_{\lambda_1, \dots, \lambda_n}(j)$. Our numerical examination of transitions between various coin defects revealed an interesting properties. When we introduce a coin defect C_n at the location n and then we slowly shift the perturbation towards the $(n+1)$ -th node, then depending on the number of stationary states corresponding to C_n we:

- (a) either manage to successfully move the localized walker – that is the case of four stationary states,
- (b) or we make the localization vanish– in case the coin defect C_n introduces only two stationary states.

Furthermore, the longer the transition is, the more successful are we in respective cases. Having four stationary states we are better at keeping the walker localized and having only two stationary states we are less likely to find the walker at the new position.

Although we are currently not able to prove that the problem of two neighbouring defects will never introduce more than four stationary states, we are able to provide strong experimental evidence that for imaginary rotations and and defects investigated by Endo and Konno (65) this is the case. For the impact of the length of passage on shifting of these defects we may see the plot of the function (146) in Figure 17. Quite a clear pattern is revealed: with increasing transition length we the function Ξ (146) grows. Ξ is certainly bounded from above by 1 for the case of preserving selected subspaces intact. Thus, the closer are we able to keep Ξ to 1, the “more” adiabatic transition we managed to pass. We thus also plot $1 - \Xi$ in logarithmic coordinates in Figure 18. Both Figure 17 and Figure 18 capture transition of the same $iR(\theta)$ coin defect.

2. We may also keep track of instantaneous projections defined as:

$$\chi_{\lambda_1, \dots, \lambda_n}(t, \psi) = \|P_{\lambda_1, \dots, \lambda_n}(t)\psi\|, \quad (147)$$

where we denote the projector onto the eigensubspaces corresponding to the eigenvalues $\lambda_1, \dots, \lambda_n$ at the time step t $P_{\lambda_1, \dots, \lambda_n}(t)$. A sample plot corresponding to the situation described in the point 1 is presented in Figure 16. While comparing the final states after having passed the adiabatic evolution depicted in Figure 16 and Figure 17, we find agreement. However the function χ (147) might not be monotonous.

We have not investigated such transition effects yet but we aim to examine their behaviour in the near future.

In order to provide deeper insight the tho problem of adiabatic transitions we aim our attention at study of multi-point defects. The analysis of adiabatic transitions, such as shifts of perturbations, shall be significantly clear as soon as we understand the spectral properties of Hadamard walks with 2 and more disturbances. Furthermore, we would like to develop a unified experimental measurement – such those outlined in (146) and (147) – of the rate of adiabaticity for discrete time evolution. It is also worth noting that the function χ (147) reveals an interesting behaviour during transitions. We have seen the relation of (147) in Figure 16. Yet we have encountered cases where “strange oscillations” occur. We shall examine these phenomena in continuation to this work.

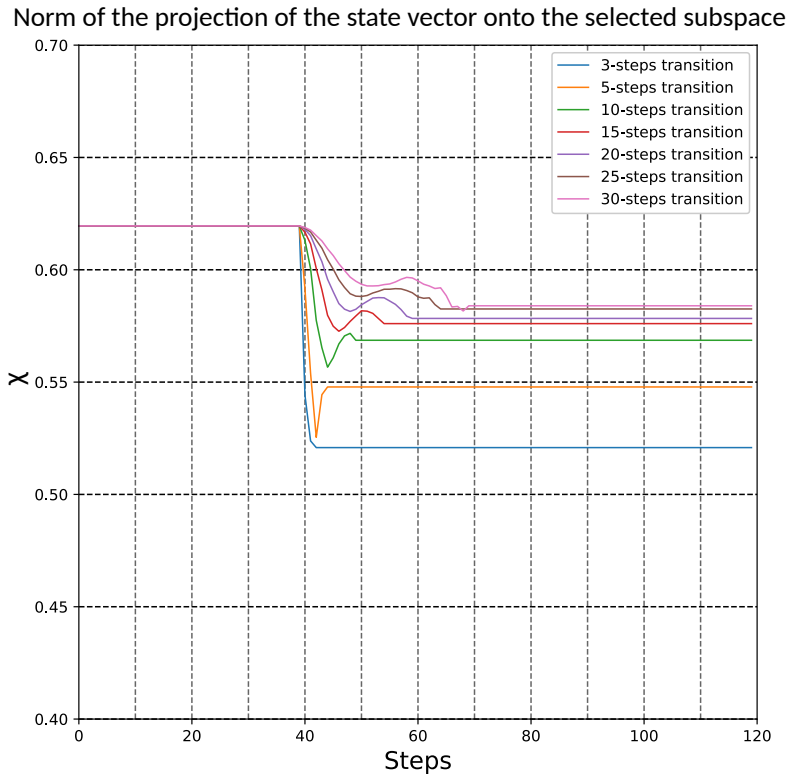


Figure 16: Comparison of transition lengths measured using the function χ (147).

Norm of the product of projections onto selected eigenspaces

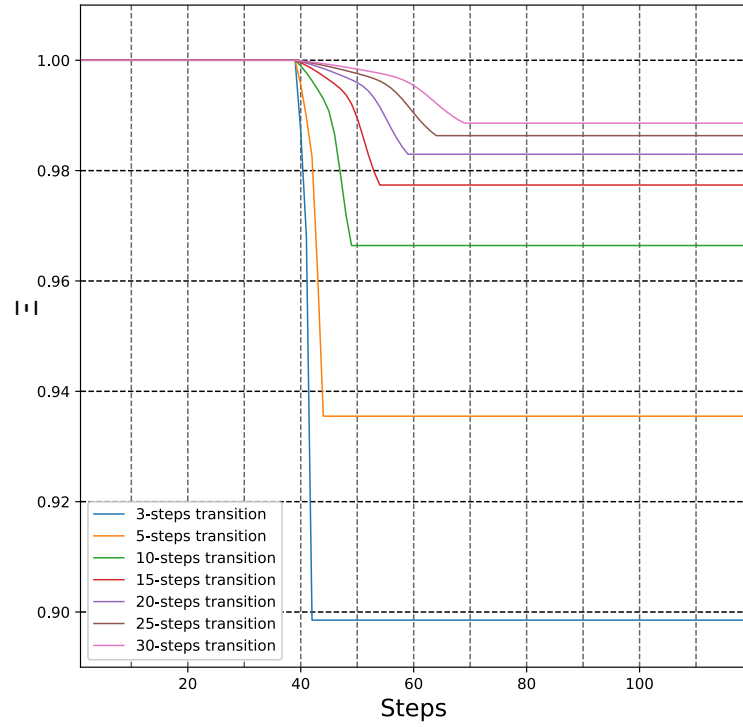


Figure 17: Comparison of different lengths of adiabatic passages. We plot the function Ξ (146) for the case of a one-node shift of the coin defect $iR(\theta)$, where $\theta = \frac{\pi}{6}$.

L^2 norm of product of projectors defective subspace:
move $i\frac{\pi}{6}$ -rotation 1 position

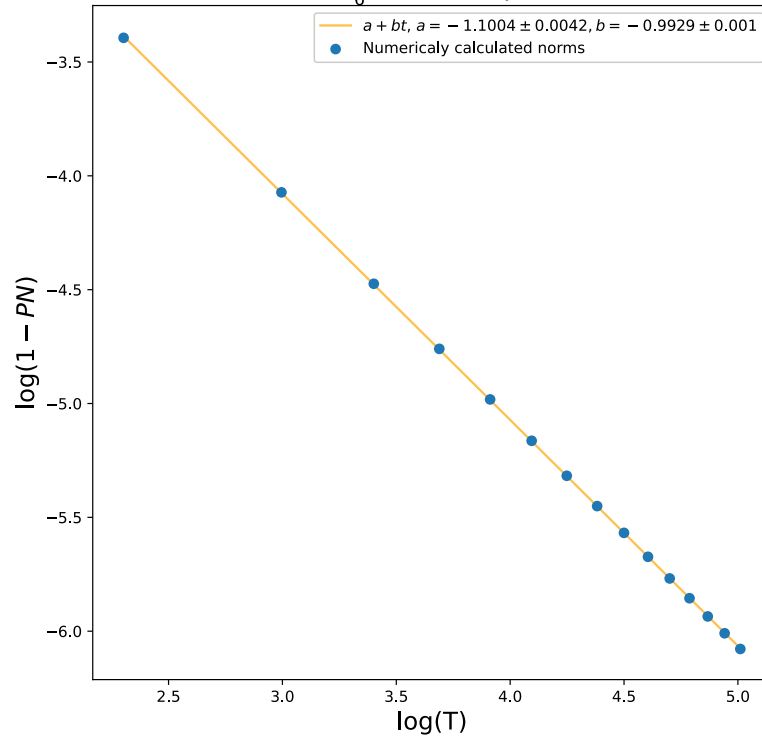


Figure 18: The probability of losing walker $\Xi - 1$ as a function of the transition times T in logarithmic axes. The fit helps us to determine the asymptotics: in this case this probability decreases as $O(\frac{1}{T})$.

4 Conclusion

We presented an analytical method uncovering solutions to the eigenvalue problem concerning Hadamard walks with a single-point defect. While investigating the stationary states, we may find zero, two or four solutions as outlined in Proposition 2.3. To our surprise, even the case concerning four roots has a relatively nice form that is expressed using the equations (123) and (124).

With the aid of our new method, the case considering phase-altered coins studied by Wójcik et al. in [2] became easy to solve. We have also revisited another well known example introduced by Endo and Konno [41]. Our results apply also in this example.

We are further interested in examination of multiple-coin defects. Right now, we are not aware of any special class of two-coin defects that might be investigated analytically. Though considering adiabatic transitions often introduces multiple perturbations at once. In order to study such transitions we had to develop own framework providing numerical solutions. We plan to develop the core of the simulator further and write an appropriate documentation, so that the code may be released. In more distant future we might consider adding a user interface.

While studying adiabatic transition we considered a trapped walker. Depending on the perturbation intermedating the trap we observed two significantly different scenarios. For defects introducing two stationary states, we are usually not able to perform state transfers. The localized state is usually dispersed to the neighbourhood of the perturbation shifted. On the other hand, experimental setups provide a strong evidence that defects with four stationary states might be transferred. Although the adiabatic theorem does not provide insight to discrete time evolution, we managed to observe phenomena similar to those from continuous realm.

A Appendix

A.1 Minor implementation details

Rather than beginning with a back end numerical simulator and equipping it with a user interface, we opted for preparing a framework-like library. Thanks to available numerical libraries NumPy [43] and SciPy [44] we opted for writing the simulator in Python. Internal routines of NumPy and SciPy and solvers therein are based on LAPACK [45] and BLAS packages (in our case FlexiBlas [46]).

Although a constructive algorithm to find paths in $U(N)$ was outlined in the section 3.1 details concerning the numerical solution was omitted. In order to perform the initial diagonalization from Proposition 3.1 must be performed. The general case requires to find all the eigenvectors of $U_2 U_1^{-1}$ and their corresponding eigenvalues. Several reliable numerical methods suitable for diagonalization of unitary matrices are available. In our case the singular values decomposition or Schur factorisation [47] offer a suitable balance between numerical precision and speed. Our implementation relies on LAPACK routines [48] provided through the interface of SciPy linear algebra package [49]. We chose the Schur decomposition for several reasons: we know the matrices to be factorized are diagonalizable and that the similarity transform is provided by a unitary matrix consisting of eigenvectors to be found. Furthermore, numerical routines used for Schur decomposition in LAPACK rely [50] on elementary Householder matrices (also known as elementary reflectors) [47]. We are thus guaranteed the eigenvectors found will form an orthonormal basis. The numerical accuracy thus gained enables us to directly implement mathematical objects introduced in the section 3.1 without need to introduce neither roundoff corrections nor renormalisation etc. Having found and stored the Schur decomposition of $U_2 U_1^{-1}$ we need to perform only two matrix multiplications in order to determine a point of the trajectory between the unitary matrices U_1 and U_2 .

Similar techniques were used in other methods and careful choice of design patterns resulted in a reliable tool providing an insight into experiments concerning quantum random walks.

A brief outline of the structure used in the program shall be presented.

We work primarily with the following objects:

1. A *state* represents a walker's state – its wavefunction in a Hilbert space coordinatized by (33).
2. A *walk* represents a non-perturbed Hadamard walk on a discrete line of desired length. This class introduces the operator of the unitary evolution and also provides methods to iterate steps of the walk. The initial position of a walker is passed as an initial state which is of the type *state*.
3. A *transition* encapsulates parameters of both diabatic and adiabatic transitions.
4. A *defect* represents a perturbed Hadamard walk derived from a parent object, where parent may be either a *walk* or a *defect*, and a transition.
5. A *record* acts as an auxiliary object to store evolution of given perturbed walks. This object is usually returned by the *record* method provided by a *defect*.

We omit the use of other classes and functions and focus on the relations between listed objects. The relations are particularly simple. Once we specify a *walk* using free parameters and an initial *state* we may ask the computer to simulate a desired number of steps while keeping track of attributes of our interest. However the main purpose of the outlined structure is to calculate adiabatic passages. We can thus initialize a walk and then set an adiabatic transition of the form (142). Then we introduce a *defect* derived from the *walk*. Our approach uses a generalised graph relations between defects. We are thus able to introduce multiple perturbations, arrange adiabatic transitions between two perturbed evolution or slowly add new defects to already perturbed evolution. Furthermore, we may track eigenvalues that arose due to defects. A piece of code will illustrate the typical use case:

```

1 import numpy as np          #imports NumPy
2 import hadam               #imports the simulator
3 init_state = state(500)
4 promenade = walk( init_state, "periodic")
5 slow_trans = transition( 100, "zig", 10, 1)
6 alpha = np.pi/4          #set the coin defect
7 factor = 1j
8 x11 = np.cos(alpha)*factor
9 x12 = np.sin(alpha)*factor
10 x21 = -np.sin(alpha)*factor
11 x22 = np.cos(alpha)*factor
12 G = [[x11, x12],[x21,x22]]
13 coinspace = defect( promenade, slow_trans, type=10, \
14                   defective=[n], coin=[G])
15 coinspace.add_another( type=10, \
16                   defective=[def_place + 4], coin=[G])
17 record = coinspace.record( 150, directory=..., make_graphs=True,
18                   graph_type="alpha-beta", check_eigenvectors=range(10, 110), \
19                   record_eigenspaces = True)
20 record.export_eigvals( file=... )

```

1. After having imported NumPy and the program itself in Python we initialize the *state*. Its size is 500 and thus it describes a state of the Hadamard walk on 250 beads. We may set other options but omitting them produces a default state that produces symmetric probability distribution for Hadamard walks.
2. A *walk* named *promenade* and a *transition* called *slow_trans* were initialised. We passed arguments: 100 steps long transition; transition function of the type (142); initial delay 10 steps and number of passafes is set to 1¹².
3. On lines 6 – 12 a perturbed coin G is set using NumPy math functions.
4. We set the target coin defects on the lines 13 and 15.
5. On line 17 we record the adiabatic transition of length 150 steps. The additional arguments specify graphing options and set ranges when to check the eigenvectors.

¹²For 2 we would perform the transition forwards and then immediately backwards. This feature gives rise to the name “zig”.

6. Finally the recorded eigenvalues are exported into a specified file.

The evolution of the program was very dynamical and tightly followed our needs. Anytime a new feature was required, we implemented it. The set of available options is thus rather lengthy and will not be presented here.

The code itself shall be released as soon as a suitable documentation becomes available.

List of Symbols and Acronyms

Symbols

\mathbb{N}	the set of positive integers $\{1, 2, \dots\}$
\mathbb{N}_0	the set of positive integers with zero $\{0, 1, 2, \dots\}$
\mathbb{Z}	integers $\{\dots, -2, -1, 0, 1, 2, \dots\}$
\widehat{N}	subset of integers $\{0, 1, 2, \dots, N\}$
\mathbb{C}	the set of complex numbers
\mathbb{R}	the set of real numbers
$\Re(z)$	the real part of a complex number z
$\Im(z)$	the imaginary part of a complex number z
$\mathbb{Z}_N = \mathbb{Z}/N\mathbb{Z}$	quotient space
$\text{Im}_F(S)$	image of the set S under a mapping F , i.e. $F(S)$
$\text{Preim}_F(S)$	preimage of the set S under a mapping F
\mathcal{H}	Hilbert space
$\text{span}\{x_1, \dots, x_n\}$	linear span
$\langle x y\rangle$	dot product of vectors x and y
$\det(A)$	determinant of A
A^T	transpose of A
A^\dagger	Hermitian transpose of A

Acronyms

AQC	adiabatic quantum computing
QA	quantum annealing
AT	adiabatic theorem

References

1. Kempe, J. Quantum random walks: an introductory overview. *Contemporary Physics* **44**, 307–327 (2003).
2. Wójcik, A. *et al.* Trapping a particle of a quantum walk on the line. *Physical Review A* **85**, 012329 (2012).
3. Spitzer, F. *Principles of random walk* (Springer Science & Business Media, 2013).
4. Papasimakis, N. & Pallikari, F. in *Complexus Mundi: Emergent Patterns in Nature* 53–62 (World Scientific, 2006).
5. Aharonov, Y., Davidovich, L. & Zagury, N. Quantum random walks. *Physical Review A* **48**, 1687 (1993).
6. Pudlák, P. *Logical foundations of mathematics and computational complexity: a gentle introduction* (Springer Science & Business Media, 2013).
7. Feynman, R. P. Simulating physics with computers. *International Journal of Theoretical Physics* **21**, 467–488 (1982).
8. Benioff, P. The computer as a physical system: A microscopic quantum mechanical Hamiltonian model of computers as represented by Turing machines. *Journal of Statistical Physics* **22** (5 May 1980).
9. Deutsch, D. Quantum Theory, the Church-Turing Principle and the Universal Quantum Computer. *Proceedings Mathematical Physical & Engineering Sciences* **400** (1818 1985).
10. Deutsch, D. Quantum Computational Networks. *Proceedings Mathematical Physical & Engineering Sciences* **425** (1868 Sept. 1989).
11. Nielsen, M. A. & Chuang, I. L. *Quantum Computation and Quantum Information* (2010).
12. Hennessy, J. L. & Patterson, D. A. *Computer architecture: a quantitative approach* (Elsevier, 2011).
13. Papadimitriou, C. H. *Computational Complexity* 1st ed. (Addison-Wesley, 1993).
14. Albash, T. & Lidar, D. A. Adiabatic quantum computation. *Reviews of Modern Physics* **90**, 015002 (2018).
15. Apolloni, B., Carvalho, C. & De Falco, D. Quantum stochastic optimization. *Stochastic Processes and their Applications* **33**, 233–244 (1989).
16. Kirkpatrick, S., Gelatt, C. D. & Vecchi, M. P. Optimization by simulated annealing. *Science* **220**, 671–680 (1983).
17. Farhi, E., Goldstone, J., Gutmann, S. & Sipser, M. Quantum computation by adiabatic evolution. *arXiv preprint quant-ph/0001106* (2000).
18. Van Dam, W., Mosca, M. & Vazirani, U. How powerful is adiabatic quantum computation?, 279–287 (2001).
19. Aharonov, D. *et al.* Adiabatic quantum computation is equivalent to standard quantum computation. *SIAM review* **50**, 755–787 (2008).

20. Childs, A. M. *et al.* Exponential algorithmic speedup by a quantum walk in *Proceedings of the thirty-fifth annual ACM symposium on Theory of computing* (2003), 59–68.
21. Ide, Y., Konno, N., Segawa, E. & Xu, X.-P. Localization of discrete time quantum walks on the glued trees. *Entropy* **16**, 1501–1514 (2014).
22. Bravyi, S., DiVincenzo, D. P., Loss, D. & Terhal, B. M. Quantum simulation of many-body Hamiltonians using perturbation theory with bounded-strength interactions. *Physical review letters* **101**, 070503 (2008).
23. Dorit Aharonov Daniel Gottesman, J. K. The Power of Quantum Systems on a Line. *Communications in Mathematical Physics* **287** (1 Apr. 2009).
24. Ehrenfest, P. Adiabatische Invarianten und Quantentheorie. *Annalen der Physik* **356**, 327–352 (1916).
25. Born, M. & Fock, V. Beweis des Adiabatsatzes. *Zeitschrift für Physik* **51**, 165–180 (1928).
26. Kato, T. On the adiabatic theorem of quantum mechanics. *Journal of the Physical Society of Japan* **5**, 435–439 (1950).
27. Marzlin, K.-P. & Sanders, B. C. Inconsistency in the application of the adiabatic theorem. *Physical Review Letters* **93**, 160408 (2004).
28. Tong, D., Singh, K., Kwek, L. C. & Oh, C. H. Quantitative conditions do not guarantee the validity of the adiabatic approximation. *Physical Review Letters* **95**, 110407 (2005).
29. Amin, M. H. S. Consistency of the Adiabatic Theorem. *Physical Review Letters* **102** (22 June 2009).
30. Messiah, A. Quantum Mechanics, Volume II. *Appedix C (Section IV North-Holland Publishing Company, Amsterdam, 1969)* (1962).
31. Ambainis, A. & Regev, O. An elementary proof of the quantum adiabatic theorem. *arXiv preprint quant-ph/0411152* (2004).
32. Jansen, S., Ruskai, M.-B. & Seiler, R. Bounds for the adiabatic approximation with applications to quantum computation. *Journal of Mathematical Physics* **48**, 102111 (2007).
33. Nenciu, G. Linear adiabatic theory. Exponential estimates. *Communications in Mathematical Physics* **152**, 479–496 (1993).
34. Elgart, A. & Hagedorn, G. A. A note on the switching adiabatic theorem. *Journal of Mathematical Physics* **53**, 102202 (2012).
35. Ge, Y., Molnár, A. & Cirac, J. I. Rapid adiabatic preparation of injective PEPS and Gibbs states, 2015. *arXiv preprint arXiv:1508.00570*.
36. Nemeč, F. Adiabatic Quantum Computing and Adiabatic Algorithm Design [unpublished research project]. <http://physics.fjfi.cvut.cz/en/cb-profile/nemecfil> (2019).
37. Biane, P., Konno, N. & Xu, Q. *Quantum potential theory* 1st ed. (Springer-Verlag Berlin Heidelberg, 2008).

38. Konno, N., Namiki, T. & Soshi, T. Symmetry of distribution for the one-dimensional Hadamard walk. *Interdisciplinary Information Sciences* **10**, 11–22 (2004).
39. Abelson, H. & Sussman, G. J. *Structure and interpretation of computer programs* (MIT Press, 1996).
40. Endo, S., Endo, T., Komatsu, T. & Konno, N. Eigenvalues of two-state quantum walks induced by the Hadamard walk. *Entropy* **22**, 127 (2020).
41. Endo, T. & Konno, N. The stationary measure of a space-inhomogeneous quantum walk on the line. arXiv: 1309.3054 [quant-ph] (2014).
42. Endo, S., Endo, T., Komatsu, T. & Konno, N. Eigenvalues of Two-State Quantum Walks Induced by the Hadamard Walk. *Entropy* **22**, 127. <http://dx.doi.org/10.3390/e22010127> (Jan. 2020).
43. Harris, C. R. *et al.* Array programming with NumPy. *Nature* **585**, 357–362. <https://doi.org/10.1038/s41586-020-2649-2> (Sept. 2020).
44. Virtanen, P. *et al.* SciPy 1.0: Fundamental Algorithms for Scientific Computing in Python. *Nature Methods* **17**, 261–272 (2020).
45. Anderson, E. *et al.* *LAPACK Users' Guide* Third (Society for Industrial and Applied Mathematics, Philadelphia, PA, 1999).
46. Köhler, M. & Saak, J. FlexiBLAS-A flexible BLAS library with runtime exchangeable backends. *LAPACK Working Notes* (2013).
47. Burden, R. L. & Faires, J. D. Numerical Analysis, Brooks. *Cole Pub* **7** (1997).
48. Blackford, S. Jan. 1991. <https://www.netlib.org/lapack/lug/node50.html>.
49. Scipy. *Numpy and Scipy Documentation* June 2020. https://github.com/scipy/scipy/blob/v1.6.3/scipy/linalg/decomp_schur.py#L17-L175.
50. Blackford, S. Jan. 1991. <https://www.netlib.org/lapack/lug/node128.html#secorthog>.